Cell Reports

Article

DOT1L regulates lipid biosynthesis and inflammatory responses in macrophages and promotes atherosclerotic plaque stability

Graphical abstract

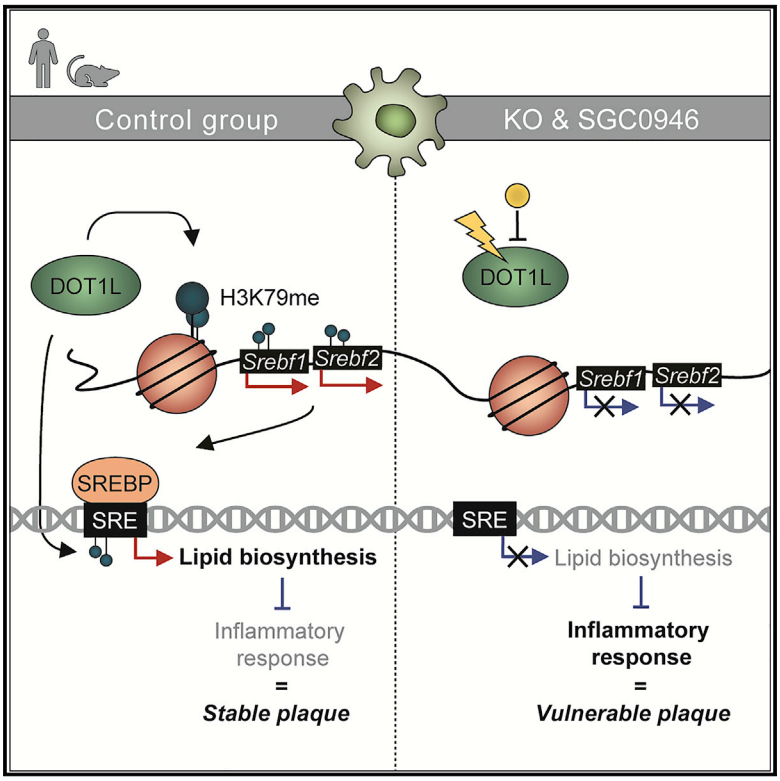

Authors

Lisa Willemsen, Koen H.M. Prange, Annette E. Neele, ..., Heinz Jacobs, Fred van Leeuwen, Menno P.J. de Winther

Correspondence

m.dewinther@amsterdamumc.nl

In brief

Willemsen et al. show that DOT1L is a crucial regulator of macrophage inflammatory responses and lipid regulatory pathways and suggest a high relevance of H3K79 methylation in inflammatory disease.

Highlights

- DOT1L inhibition leads to macrophage hyperactivation
- DOT1L directly regulates macrophage lipid biosynthesis gene programs
- Myeloid *Dot1l* deficiency reduces atherosclerotic plaque stability
- Myeloid *Dot1l* deficiency increases the activation of inflammatory plaque macrophages

Willemsen et al., 2022, Cell Reports *41*, 111703
November 22, 2022
https://doi.org/10.1016/j.celrep.2022.111703

CellPress

Cell Reports

CellPress
OPEN ACCESS

Article

DOT1L regulates lipid biosynthesis and inflammatory responses in macrophages and promotes atherosclerotic plaque stability

Lisa Willemsen,[1] Koen H.M. Prange,[1] Annette E. Neele,[1] Cindy P.A.A. van Roomen,[1] Marion Gijbels,[1,2] Guillermo R. Griffith,[1] Myrthe den Toom,[1] Linda Beckers,[1] Ricky Siebeler,[1] Nathanael J. Spann,[3] Hung-Jen Chen,[1] Laura A. Bosmans,[1] Andrej Gorbatenko,[1] Suzanne van Wouw,[1] Noam Zelcer,[1] Heinz Jacobs,[4] Fred van Leeuwen,[5,6] and Menno P.J. de Winther[1,7,*]

[1]Department of Medical Biochemistry, Experimental Vascular Biology, Amsterdam Cardiovascular Sciences, Amsterdam Infection and Immunity, Amsterdam UMC, University of Amsterdam, 1105 AZ Amsterdam, the Netherlands
[2]Department of Pathology CARIM, Cardiovascular Research Institute Maastricht, GROW-School for Oncology and Developmental Biology, Maastricht University, Maastricht, the Netherlands
[3]Department of Cellular and Molecular Medicine, University of California, San Diego, 9500 Gilman Drive, La Jolla, CA 92093-0651, USA
[4]Division of Tumor Biology & Immunology, Netherlands Cancer Institute, 1066 CX Amsterdam, the Netherlands
[5]Division of Gene Regulation, Netherlands Cancer Institute, 1066 CX Amsterdam, the Netherlands
[6]Department of Medical Biology, Amsterdam UMC, University of Amsterdam, 1105 AZ Amsterdam, the Netherlands
[7]Lead contact
*Correspondence: m.dewinther@amsterdamumc.nl
https://doi.org/10.1016/j.celrep.2022.111703

SUMMARY

Macrophages are critical immune cells in inflammatory diseases, and their differentiation and function are tightly regulated by histone modifications. H3K79 methylation is a histone modification associated with active gene expression, and DOT1L is the only histone methyltransferase for H3K79. Here we determine the role of DOT1L in macrophages by applying a selective DOT1L inhibitor in mouse and human macrophages and using myeloid-specific *Dot1l*-deficient mice. We found that DOT1L directly regulates macrophage function by controlling lipid biosynthesis gene programs including central lipid regulators like sterol regulatory element-binding proteins SREBP1 and SREBP2. DOT1L inhibition also leads to macrophage hyperactivation, which is associated with disrupted SREBP pathways. *In vivo*, myeloid *Dot1l* deficiency reduces atherosclerotic plaque stability and increases the activation of inflammatory plaque macrophages. Our data show that DOT1L is a crucial regulator of macrophage inflammatory responses and lipid regulatory pathways and suggest a high relevance of H3K79 methylation in inflammatory disease.

INTRODUCTION

Macrophages are essential cells of the innate immune system that exhibit high plasticity and perform various tissue-specific functions.[1] In chronic inflammatory disease, like atherosclerosis, many macrophage activation states are observed, and these contribute to both the initiation and progression of the disease. Cardiovascular disease remains the leading cause of death worldwide with atherosclerosis as the main underlying cause.[2] The atherosclerotic microenvironment is diverse and drives a range of macrophage phenotypes.[3] Within the atherosclerotic plaque, pro-inflammatory macrophages promote local inflammation and contribute to vascular injury and matrix degradation, and they are therefore associated with disease progression and plaque destabilization.[4] Anti-inflammatory macrophages secrete mediators that suppress inflammation and promote tissue remodeling and repair through collagen formation and scavenging of debris and dead cells.[2,3]

Macrophage differentiation and function are tightly controlled by transcriptional and epigenetic alterations.[5,6] During macrophage differentiation and activation, epigenetic modulators regulate histone modifications, e.g., acetylation and methylation, that influence chromatin accessibility and RNA polymerase II recruitment, and thereby control the transcriptional repertoire of cells.[7] Targeting macrophage epigenetic modulators can be applied to guide macrophage activation in the right direction for a beneficial therapeutic outcome.[8,9]

Disruptor of telomeric silencing-1-like (DOT1L) is the only known methyltransferase for histone 3 lysine 79 (H3K79) and is evolutionarily conserved.[10] H3K79 di- and trimethylation modifications are mainly found in the body of active genes and are associated with gene transcription.[11–13] DOT1L has been extensively studied in cancer and is a therapeutic target for treating MLL-rearranged leukemia.[14] Completed phase 1 clinical trials show that DOT1L inhibitor pinometostat (EPZ-5676) has an acceptable safety profile in children and adults with relapsed or refractory MLL-rearranged leukemia.[15,16] Furthermore,

DOT1L controls T and B cell differentiation and responses,[17–20] prevents premature differentiation toward antigen inexperienced memory-like CD8+ T cells,[17] is essential for appropriate localization of B cells to form germinal centers, and DOT1L deficiency prohibits differentiation of germinal center B cells.[18,19] However, the function of DOT1L in macrophage physiology remains poorly understood.

Here we report the role of DOT1L in macrophages *in vitro* and *in vivo* by applying a selective DOT1L inhibitor on mouse and human macrophages and using myeloid-specific *Dot1l*-deficient mice. DOT1L inhibition results in hyperinflammatory macrophages with defective cholesterol and fatty acid synthesis gene programs. DOT1L mediates H3K79 methylation of genes that are involved in the synthesis of cholesterol and fatty acids, including master regulators *Srebf1* and *Srebf2*. Consequently, suppressed cholesterol and fatty acids pathways program a hyperinflammatory state in macrophages particularly characterized by enhanced IFN signaling. In an *in vivo* model for atherosclerosis, myeloid *Dot1l* deficiency aggravates chronic inflammatory disease by increasing the activation of inflammatory plaque macrophages and contributing to an unstable, exacerbated plaque phenotype. Overall, our study provides essential insights into the molecular mechanisms that control inflammatory responses in human disease. This will be instrumental in furthering our understanding of the pathogenesis of diseases like atherosclerosis and cancer. Our insights also reveal epigenetic processes controlling disease that are relevant for therapeutic purposes and should be taken into account when DOT1L-targeting therapy is considered.

RESULTS

DOT1L activates cholesterol synthesis in mouse macrophages

To understand the function of DOT1L in macrophage physiology, we applied a potent and selective DOT1L inhibitor (SGC0946) to mouse macrophages.[21] Murine bone marrow cells were differentiated to macrophages (BMDMs) in the presence of SGC0946 or DMSO starting at different time points (Figure 1A). Since DOT1L is the only known H3K79 methyltransferase, we measured H3K79me2 to determine the functional effect of DOT1L inhibition. Although short incubation with SGC0946 already significantly reduced H3K79me2, DOT1L inhibition from the initiation of macrophage differentiation resulted in the most pronounced H3K79me2 reduction (Figures 1B and S1A). Therefore, in subsequent experiments, we inhibited DOT1L from the onset of differentiation. SGC0946 treatment did not affect BMDM viability, yield, or expression of the macrophage differentiation surface markers F4/80 and CD11b and transcriptional markers (*Csf1*, *Csf1r*, *Mafb*, *Mertk*, and *Adgre1*), indicating that macrophage differentiation is not affected (Figures S1B–S1E). RNA-seq revealed that the expression of 551 genes was significantly downregulated, and 611 genes were upregulated after SGC0946 treatment in BMDMs (FDR < 0.05; Figure S1F). Interestingly, the top downregulated pathway was "Sterol biosynthetic process," indicating disruption of cellular metabolic pathways, while "Regulation of cell adhesion" was the most upregulated pathway (Figure 1C). Gene set enrichment analysis (GSEA) further confirmed the significant enrichment of sterol biosynthetic-related gene expression in DMSO compared with SGC0946-treated BMDMs (Figure S1G). The sterol biosynthetic process pathway mainly consists of genes regulating cholesterol synthesis. We indeed found suppression of key genes encoding enzymes regulating cholesterol synthesis like 3-hydroxy-3-methylglutaryl-CoA synthase 1 (*Hmgcs1*), mevalonate kinase (*Mvk*), squalene epoxidase (*Sqle*), lanosterol synthase (*Lss*), 24-dehydrocholesterol reductase (*Dhcr24*), and 3-hydroxy-3-methylglutaryl coenzyme A (HMG-CoA) reductase (*Hmgcr*), the rate-limiting enzyme of cholesterol synthesis (Figures 1D and 1E). To conclude, DOT1L inhibition particularly suppresses cholesterol biosynthetic pathways in macrophages.

DOT1L-mediated H3K79 methylation correlates with gene activity in macrophages

To understand how DOT1L inhibition results in suppressed cholesterol synthesis in macrophages, we performed ChIP-seq for H3K79me2 in BMDMs. We found that in macrophages, H3K79me2 was predominantly localized at the regions downstream of transcription start sites, and the H3K79me2 signal was significantly lower after SGC0946 treatment (Figure 2A). Under normal conditions, H3K79me2 was present at 51.7% ± 0.46% (10,665/20,621) of the mouse protein-coding genes in BMDMs. Additionally, the average of 21,993 ± 437 H3K79me2 identified peaks marking 10,665 ± 90 unique genes dropped significantly to 14,202 ± 895 marking 7,012 ± 489 genes after SGC0946 treatment (Figures S2A and S2B). Next, we assessed the correlation between gene expression and H3K79me2 levels. Therefore, we combined the H3K79me2 ChIP-seq data with the RNA-seq data of DMSO- and SGC0946-treated BMDMs (Figure 2B). This revealed an inverse correlation between changes in gene expression after DOT1L inhibition and basal levels of gene expression, as described.[13] Genes that were upregulated after SGC0946 treatment had lower basal gene expression levels, whereas genes downregulated by SGC0946 had higher basal gene expression levels (Figure 2B, left, and Figure 2C). Moreover, high basal H3K79me2 was a key characteristic of genes that were transcriptionally suppressed by SGC0946, while genes that were upregulated or not affected had lower levels of H3K79me2 (Figure 2B, right, and Figure 2D). Thus, H3K79me2 occupancy correlates nicely with gene activity in macrophages, and as described in B cells and T cells, inhibition of DOT1L particularly affects highly expressed genes with high levels of H3K79me2.[17,18,20]

DOT1L controls cholesterol and fatty acid synthesis in macrophages directly and indirectly via *Srebf1* and *Srebf2* H3K79 methylation

Given that DOT1L-mediated H3K79me2 correlates with gene activity,[13] genes that are downregulated after DOT1L inhibition are likely to include direct targets of DOT1L. The combined H3K79me2 ChIP-seq data with the RNA-seq data of DMSO- and SGC0946-treated BMDMs also showed that transcriptionally downregulated genes (FDR < 0.05) with high H3K79me2 levels (>100) are strongly enriched for "Sterol biosynthetic process" and "Positive regulation of lipid biosynthetic process" (Figure S2C). The latter also includes fatty acid biosynthesis, and indeed, fatty acid synthesis-regulating genes, including fatty

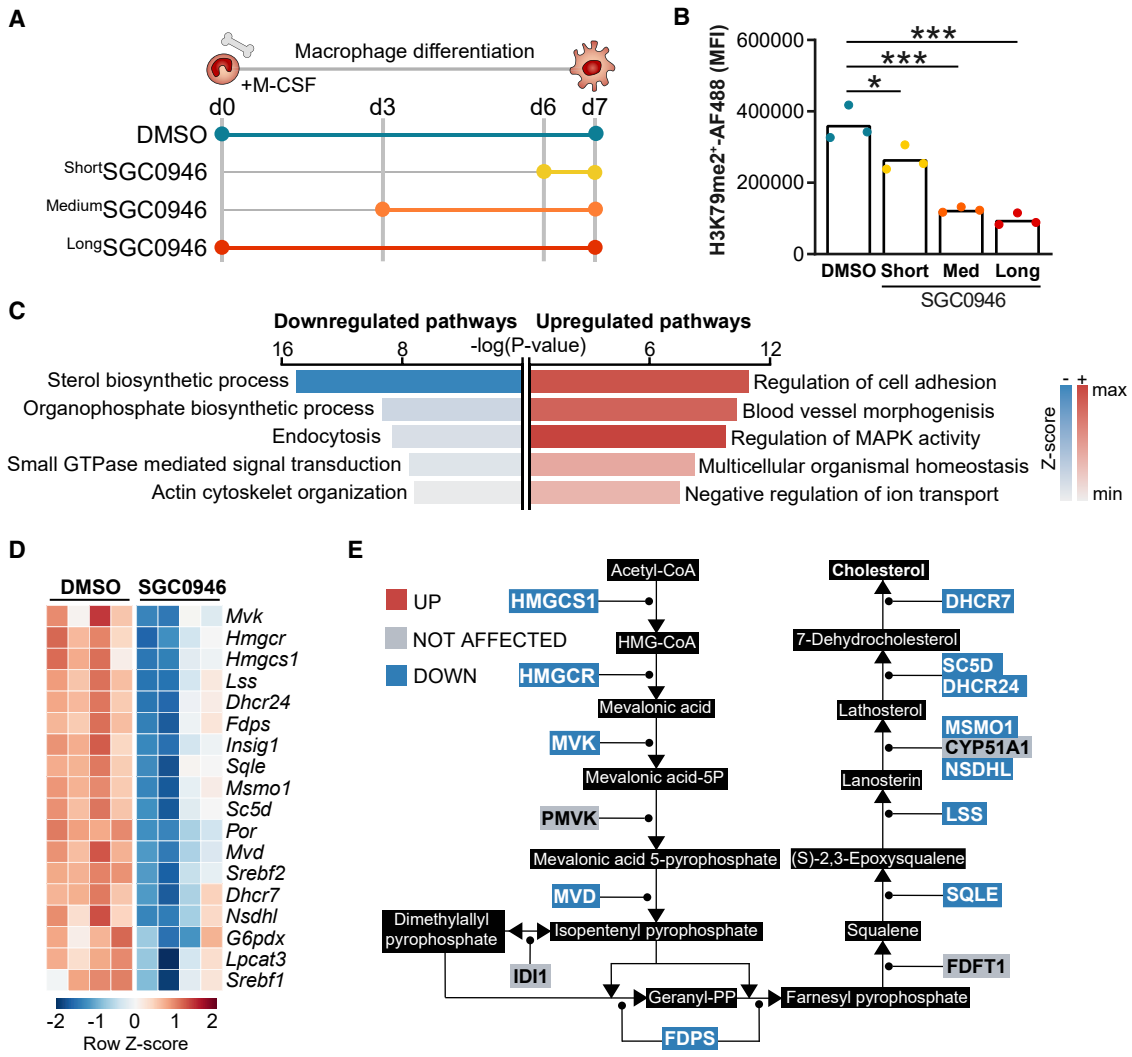

Figure 1. DOT1L regulates cholesterol synthesis in mouse macrophages

(A) DOT1L was inhibited by SGC0946 during bone marrow to macrophage differentiation at different time points (from day 0, 3, or 6). DMSO was used as a control.

(B) H3K79 dimethylation levels were measured in SGC0946-treated BMDMs. n = 3 biological replicates per group. *p = 0.0147, ***p < 0.001 by ordinary one-way ANOVA with Dunnett's method.

(C) Top five downregulated and upregulated pathways of the Gene Ontology pathway analysis of differentially expressed genes (FDR < 0.05) between SGC0946- and DMSO-treated BMDMs.

(D) Heatmap indicating the row *Z* score of genes of the pathway sterol biosynthetic process that are significantly downregulated in SGC0946- and DMSO-treated BMDMs.

(E) Gene expression changes of the enzymes regulating the cholesterol biosynthesis pathway after SGC0946 treatment in BMDMs. (C–E) n = 4 biological replicates per group.

acid desaturase 1 (*Fads1*), fatty acid elongases (*Elov5*, *Elov6*), acyl-CoA synthetase long-chain family member 3 (*Acsl3*), and the rate-limiting enzyme of the fatty acid synthesis acetyl-CoA carboxylase (*Acaca*), were downregulated by DOT1L inhibition (Figure S2D). Moreover, GSEA further confirmed the significant enrichment of fatty acid biosynthesis-related gene expression in DMSO- compared with SGC0946-treated BMDMs (Figure S2E). In line, H3K79me2 levels of genes encoding critical enzymes of the cholesterol and fatty acid biosynthesis pathways, like *Lss*, *Dhcr24*, and *Acaca,* were relatively high in DMSO-treated BMDMs and dropped significantly after SGC0946 treatment (Figure S2F). Therefore, the suppressed cholesterol and fatty acid synthesis phenotype observed after SGC0946 treatment can be explained by direct H3K79me2 hypomethylation of genes encoding for the enzymes in these pathways. Next to that, upstream regulator analysis identified the sterol regulatory element-binding transcription factors (*Srebf1* and *Srebf2*) as the most significantly suppressed transcriptional regulators after SGC0946 treatment (Figure 2E). SREBP1 and SREBP2 are master regulators of fatty acid and cholesterol synthesis, respectively.[22] *Srebf1* and *Srebf2* gene expression and H3K79me2 levels were indeed significantly reduced after SGC0946 treatment (Figures 2F and 2G). Nuclear

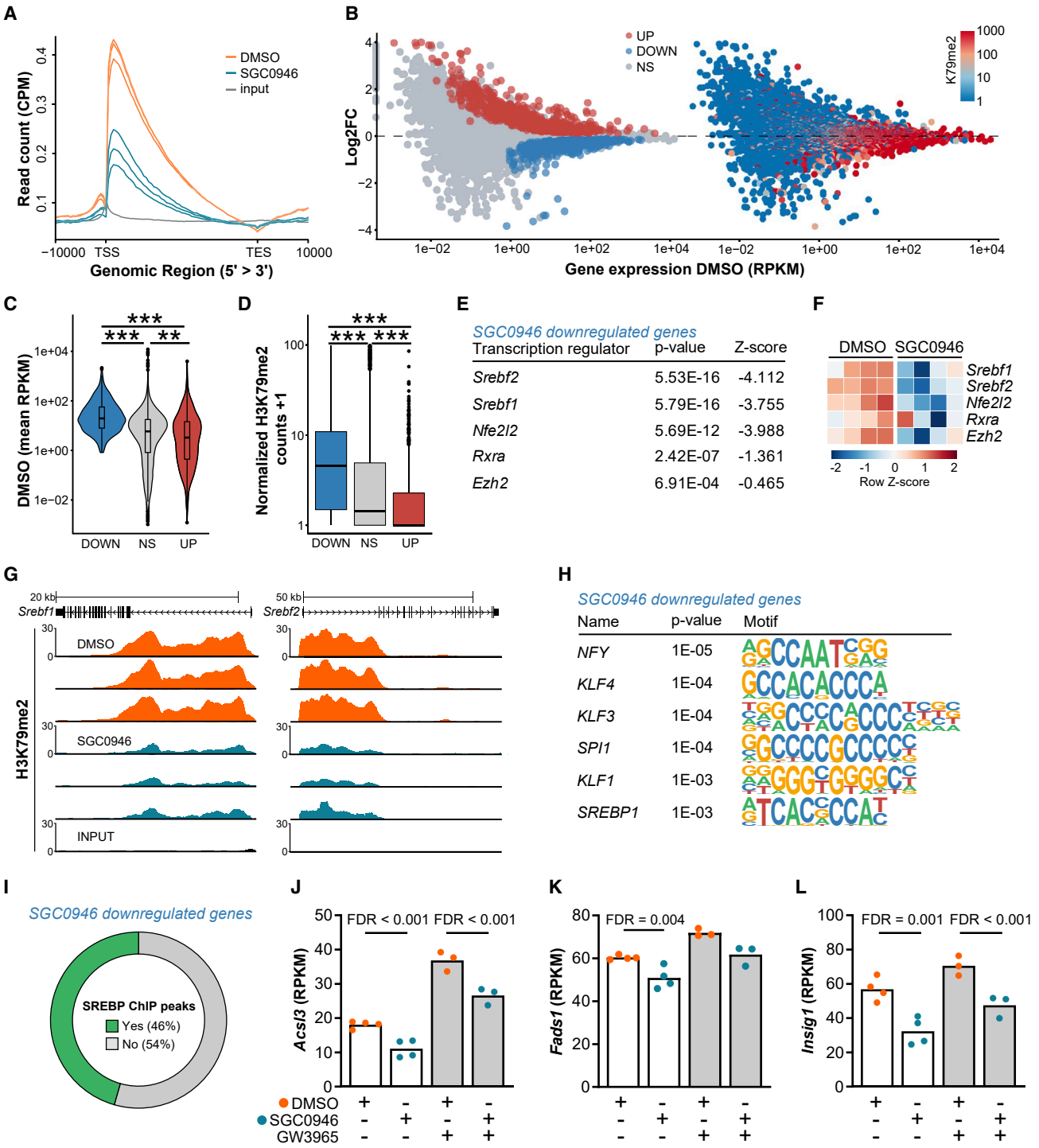

Figure 2. DOT1L-mediated H3K79 methylation correlates with gene activity and controls cholesterol synthesis directly and indirectly via *Srebf1* and *Srebf2* methylation in macrophages

(A) Genomic distribution of H3K79me2 levels determined by ChIP-seq in DMSO- and SGC0946-treated BMDMs.

(B) Gene expression levels (RPKM) of DMSO-treated BMDMs versus $\log_2$ ratios of the gene expression of SGC0946/DMSO-treated BMDMs with as a third dimension the upregulated genes in red and downregulated genes in blue (FDR < 0.05; left) and normalized H3K79me2 expression of DMSO-treated BMDMs (right).

(C) Gene expression levels (RPKM) of DMSO-treated BMDMs of genes that are downregulated (blue), not differentially expressed (gray), or upregulated (red) after SGC0946 treatment.

(legend continued on next page)

SREBP2 protein expression was also reduced after SGC0946 treatment (Figure S2G). Additionally, motif enrichment analysis identified SREBP1 and its transcriptional binding partner NFY as the most enriched motifs among the transcriptionally downregulated genes (Figure 2H).[23] Interestingly, ChIP-seq analyses revealed that SREBP1/2 directly interacts with 46% of the genes that are downregulated by SGC0946 treatment (p value for enrichment < 0.00, Figure 2I), including *Sc5d*, *Msmo1*, and *Mvd* (Figures 1D and S2H). This indicates that almost half of the genes regulated by DOT1L are also regulated by SREBP1/2. So, in addition to the direct effects of SGC0946 leading to H3K79me2 hypomethylation of genes in the cholesterol and fatty acid synthesis pathways, H3K79me2 hypomethylation and subsequently reduced gene expression of *Srebf1* and *Srebf2* further downregulate cholesterol and fatty acid synthesis pathways indirectly.

Srebf1 is a known liver X receptor (LXR) target gene,[24] and LXR is a central regulator of metabolism. We applied an LXR agonist (GW3965) to test whether *Srebf1* induction is blocked by SGC0946 treatment in macrophages. Indeed, LXR activation induced the transcription of different lipid metabolism genes that were downregulated after DOT1L inhibition like *Acsl3*, *Fads1*, insulin-induced gene 1 (*Insig1)*, and *Srebf1* (Figures 2J–2L and S2I). While combined treatment of GW3965 with SGC0946 resulted in upregulation of these genes, SGC0946 treatment still significantly reduced the level of induction confirming that reduced *Srebf1* expression after SGC0946 treatment might indeed be contributing to the suppression of lipid metabolism-related DOT1L target genes. Moreover, LXR activation suppressed the transcription of *Srebf2,* but the differences between DMSO- and SGC0946-treated BMDMs remained after GW3965 treatment (Figure S2J). These data illustrate that transcription factor activation and H3K79 methylation act separately on gene expression but synergistically enhance gene transcription.

DOT1L inhibition results in hyperinflammatory macrophages

Macrophages play a central role in the orchestration of inflammation. Therefore, the role of DOT1L in regulating the inflammatory response of BMDMs was evaluated after TLR4 activation by LPS. RNA-seq analysis of LPS-activated BMDMs treated with SGC0946 revealed that the expression of 361 genes was upregulated and that of 223 genes was downregulated by DOT1L inhibition (Figure S3A). The upregulated genes are involved in ''Regulation of cell adhesion'' and ''Inflammatory response,'' while the downregulated genes again showed that the ''Cholesterol metabolic process'' was suppressed after SGC0946 treatment (Figure 3A). GSEA confirmed that SGC0946 treatment resulted in a gene signature that is highly similar to the gene set "Inflammatory response'' (Figure 3B). The hyperinflammatory effect of DOT1L inhibition was confirmed by the substantial overlap (62%) of LPS-induced genes and the genes further amplified by SGC0946 (Figure 3C). This overlap contained many important regulators of the inflammatory response, including chemokines (*Ccl6, Cxcl9, Cxcl11*) and their receptors (*Ccr1*, *Ccr5*), cytokines (*Il12a, Tnfsf10*), Fc-gamma receptors (*Fcgr2b, Fcgr4*), class II major histocompatibility complex transactivator (*Ciita*), interferon-related transcripts (*Ifi213, Ifi44, Ifit1bl1, Irf8, Mx2, Oasl1*), and matrix metalloproteases (*Mmp13*, *Mmp25*; Figure 3D). Furthermore, flow cytometry showed that SGC0946-treated BMDMs had higher surface marker expression of costimulatory molecule CD86, Fc-gamma receptor Ia (CD64), and MHCII after activation (Figures 3E–3G and S3B–S3D). Thus, DOT1L inhibition induces a hyperresponsive macrophage state.

The hyperinflammatory macrophage phenotype is linked to a downregulation of SREBPs

Given that H3K79 methylation is a marker of active gene expression, LPS-induced genes that are enhanced by DOT1L inhibition are unlikely direct targets of DOT1L (Figures 2B–2D). To identify candidate direct and indirect target genes that could explain the hyperinflammatory macrophage phenotype in DOT1L-inhibited macrophages, we performed upstream regulator analysis. First, genes that were upregulated by SGC0946 were used to identify indirect targets. Upstream regulator analysis showed that IFN-γ, LPS, STAT1, and NF-κB are (indirect) mediators of the hyperinflammatory state that is induced after SGC0946 treatment (Figure 3H). IFN-related enriched motifs (interferon regulatory factors and interferon-sensitive response element) were enriched in upregulated genes, which shows that hyperactivation is mainly driven by enhanced IFN signaling upon DOT1L inhibition (Figure 3I). This was confirmed by increased IFN-β production after SGC0946 treatment (Figure 3J).

Second, genes that were suppressed after SGC0946 treatment were used to identify direct targets of DOT1L. Upstream regulator analysis showed that downregulation of *Srebf1* and *Srebf2* is associated with the suppressed gene expression profile of SGC0946- and LPS-treated BMDMs (Figure 4A). Interestingly, York et al. targeted either *Srebf1* or *Srebf2* using shRNA in THP-1 cells and showed that limiting cholesterol synthesis enhances type I IFN signaling. Genes that were upregulated after SGC0946 treatment were indeed significantly enriched in shSREBP1 and shSREBP2 versus control shRNA-treated THP-1

(D) Normalized H3K79me2 counts + 1 of DMSO-treated BMDMs of genes that are downregulated (blue), not differentially expressed (gray), or upregulated (red) after SGC0946 treatment. Boxplots show median values (center lines), interquartile ranges (IQRs; box edges), whiskers extending to the most extreme points within the range between the lower quantile negative (1.5 × IQR) and lower quantile positive (1.5 × IQR), and outliers are indicated as dots.
(E) Top five downregulated upstream regulators of the upstream regulator analysis of the Ingenuity Pathway Analysis (IPA) software. Transcriptional regulators with a negative activation *Z* score and significantly downregulated gene expression (FDR < 0.05) were selected.
(F) Heatmap containing the gene expression (row *Z* score) of the top five upstream regulators.
(G) UCSC browser captures of H3K79me2 levels on *Srebf1* and *Srebf2* of DMSO- and SGC0946-treated BMDMs.
(H) HOMER known motif enrichment analysis on the genes that were downregulated (FDR < 0.05) after SGC0946 treatment in BMDMs.
(I) Pie chart showing the overlap of the genes downregulated by SGC0946 and SREBP1/2 ChIP-seq peaks.
(J) *Acsl3*, (K) *Fads1*, and (L) *Insig1* mRNA expression in SGC0946- or control-treated BMDMs incubated with LXR agonist GW3965 (2 μM) or control for 17 h. H3K79me2 ChIP-seq: n = 3 biological replicates per group. RNA-seq: n = 4 biological replicates per group (n = 3 for GW3965). (C and D) **p < 0.01, ***p < 0.001 by ordinary one-way ANOVA with Dunnett's method.

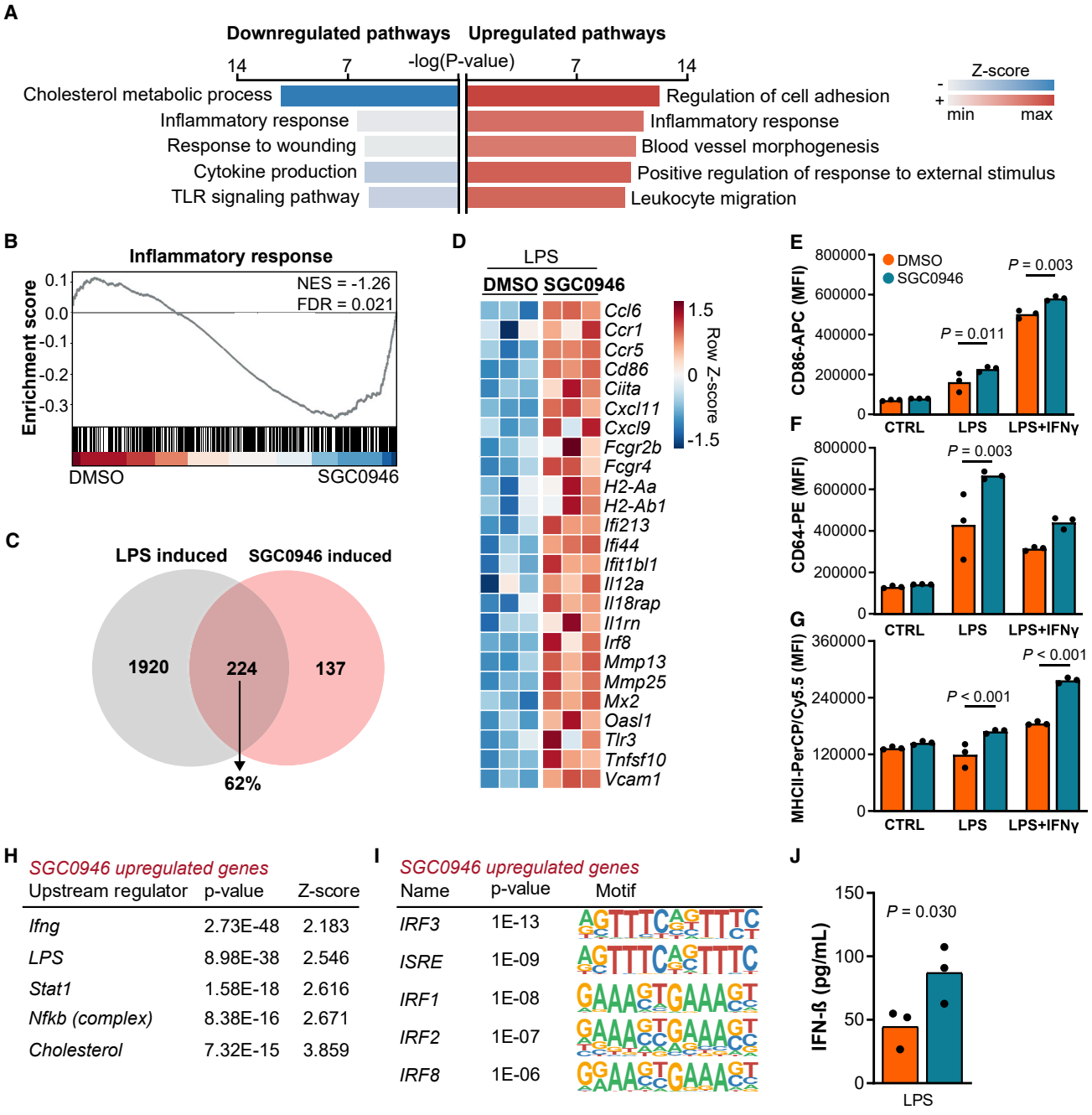

H

SGC0946 upregulated genes

Upstream regulator	p-value	Z-score
Ifng	2.73E-48	2.183
LPS	8.98E-38	2.546
Stat1	1.58E-18	2.616
Nfkb (complex)	8.38E-16	2.671
Cholesterol	7.32E-15	3.859

I

SGC0946 upregulated genes

Name	p-value	Motif
IRF3	1E-13	
ISRE	1E-09	
IRF1	1E-08	
IRF2	1E-07	
IRF8	1E-06	

Figure 3. DOT1L inhibition results in hyperinflammatory macrophages

(A) Top five downregulated and upregulated pathways of the Gene Ontology pathway analysis of differentially expressed genes (FDR < 0.05) between SGC0946- and DMSO-treated BMDMs stimulated with LPS for 3 h.

(B) Gene set enrichment analysis (GSEA) of the Gene Ontology inflammatory response pathway (GO: 0006954) on the gene expression profiles of DMSO- and SGC0946 treated BMDMs.

(C) Venn diagram showing the overlap of SGC0946-induced genes and genes that were induced by TLR4 activation with LPS.

(D) Heatmap indicating the row *Z* score of numerous pro-inflammatory genes in SGC0946-treated BMDMs after 3 h LPS stimulation.

(E–G) Protein surface expression of CD86 (E), CD64 (F), or MHCII (G) on SGC0946- and DMSO-treated BMDMs after either 24 h of control, LPS, or LPS + IFN-γ exposure.

(H) Top five upregulated regulators of the upstream regulator analysis that was performed using the Ingenuity Pathway Analysis (IPA) software.

(I) HOMER known motif enrichment analysis on the genes that were upregulated (FDR < 0.05) after SGC0946 treatment in LPS-activated BMDMs.

(J) IFN-β production in the supernatant of DMSO- or SGC0946-treated BMDMs that were activated with LPS for 3 h. p value was calculated using a two-tailed unpaired t test. (A–J) n = 3 biological replicates per group. (E–G) p values were calculated by two-way ANOVA with Šidák correction.

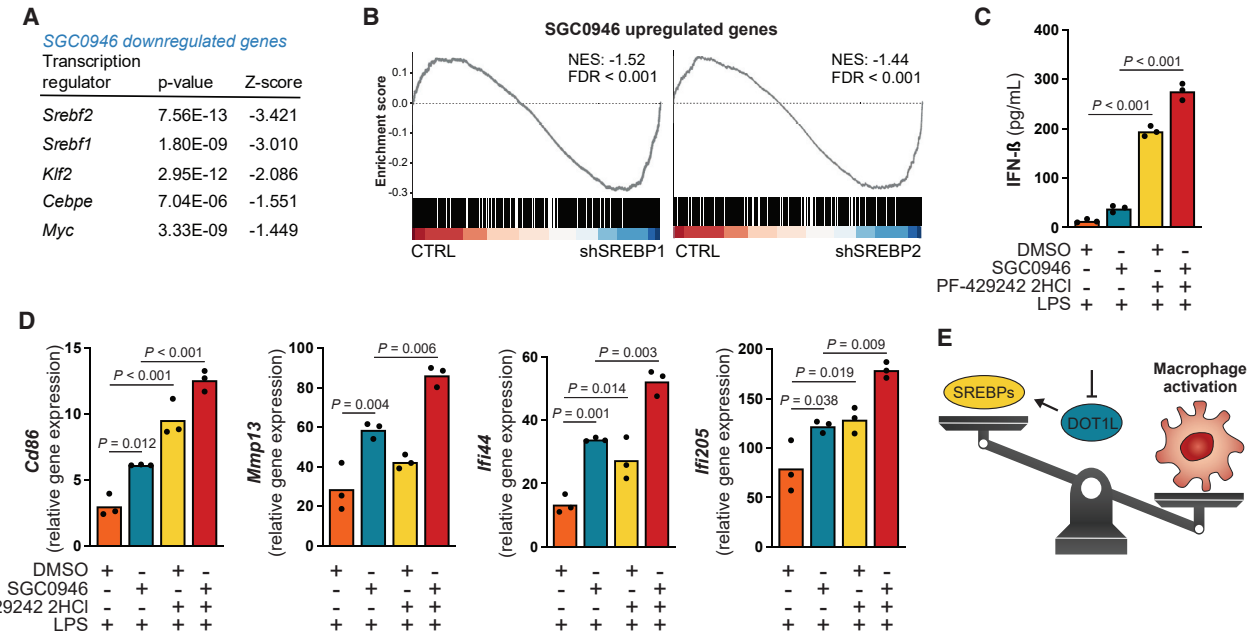

Figure 4. SREBP inhibition increases macrophage inflammatory responses

(A) Top five downregulated transcription regulators of the IPA upstream regulator analysis.

(B) GSEA of the genes that are upregulated by SGC0946 in BMDMs on the publicly available dataset (GEO: GSE73942): control versus shSREBP1 (left) and shSREBP2 (right) THP-1 cells.

(C) IFN-β production in the supernatant of BMDMs that were activated on day 8 with LPS for 24 h. 10 μM PF-429242 dihydrochloride was added on day 7 to inhibit SREBP S1P for 24 h.

(D) mRNA expression of the *Cd86*, *Mmp13*, *Ifi44*, and *Ifi205* of BMDMs that were activated with LPS for 3 h was measured using qPCR. (A–D) n = 3 biological replicates per group. (C and D) p values were calculated by ordinary one-way ANOVA with a Tukey's multiple comparison test.

(E) Schematic for the proposed mechanism of how DOT1L inhibition could result in macrophage activation via SREBP suppression.

cells (Figure 4B).[25] Upregulated and enriched genes included classical interferon-regulated genes like *Ifi213*, *Ifi44*, *Ifit1bl1*, *Irf8*, *Mx2*, and *Oasl1* (Figure 3D). To confirm that inhibition of SREBPs results in upregulation of the inflammatory response in macrophages, their prerequisite proteolytic activation was inhibited using the site-1 protease (S1P) inhibitor PF-429242 dihydrochloride. SREBP inhibition significantly increased IFN-β secretion (Figure 4C) and upregulated the expression of inflammatory genes such as *Cd86*, *Mmp13*, *Ifi44*, and *Ifi205* in BMDMs compared with DMSO (Figure 4D). These genes were also significantly upregulated after SGC0946 treatment, and interestingly, administrating both SGC0946 and PF-429242 dihydrochloride resulted in an additive effect. Thus, hyperinflammatory macrophage activation by DOT1L inhibition is probably linked to the suppression of *Srebf1* and *Srebf2*. In conclusion, our data suggest a pathway where inhibition of DOT1L activity leads to suppressed SREBP lipid synthetic pathways that consequently enhance macrophage inflammatory activation (Figure 4E).

DOT1L suppression inhibits cholesterol synthesis and induces a hyperinflammatory state in human macrophages

We next assessed the human relevance of the DOT1L-dependent macrophage phenotype we observed in mice. SGC0946-treated human monocyte-derived macrophages (hMDMs) were characterized by RNA-seq and cytokine analysis, either under unstimulated conditions or LPS-induced activation. The expression of 450 and 436 genes was downregulated and that of 565 and 512 genes was upregulated after SGC0946 treatment only or combined with LPS activation, respectively (Figures 5A and 5B). Under unstimulated conditions, pathway analysis reveals that SGC0946 treatment in hMDMs results in a suppressed "Cholesterol biosynthetic process" pathway and upregulation of numerous inflammatory pathways (Figure 5C). Again, key rate-limiting enzymes of the cholesterol biosynthesis pathway were significantly downregulated by DOT1L inhibition (Figure 5D). After TLR4 stimulation, pathway analysis showed that SGC0946-treated hMDMs were more activated (Figure 5E), corroborated by enhanced expression of relevant pro-inflammatory mediators like *Il12b*, *Il6*, and *Il1a* (Figure 5B). Moreover, cytokine secretion assays showed that SGC0946 treated hMDMs produced more IL-12p40, IL-6, IL-8, and IL-1β after activation (Figures 5F–5I). Thus, DOT1L inhibition suppresses cholesterol biosynthesis and enhances inflammatory activation in human macrophages.

Myeloid-specific *Dot1l* deletion affects macrophage inflammatory responses and cholesterol regulation in mice

To understand the importance of DOT1L in macrophage physiology *in vivo*, we generated myeloid-specific knockouts for DOT1L, i.e., *LysMcre*$^{-}$*Dot1l*$^{fl/f}$ (WT) and *LysMcre*$^{+}$*Dotl*$^{fl/fl}$ (KO; Figure 6A) by employing a mouse model in which exon 2

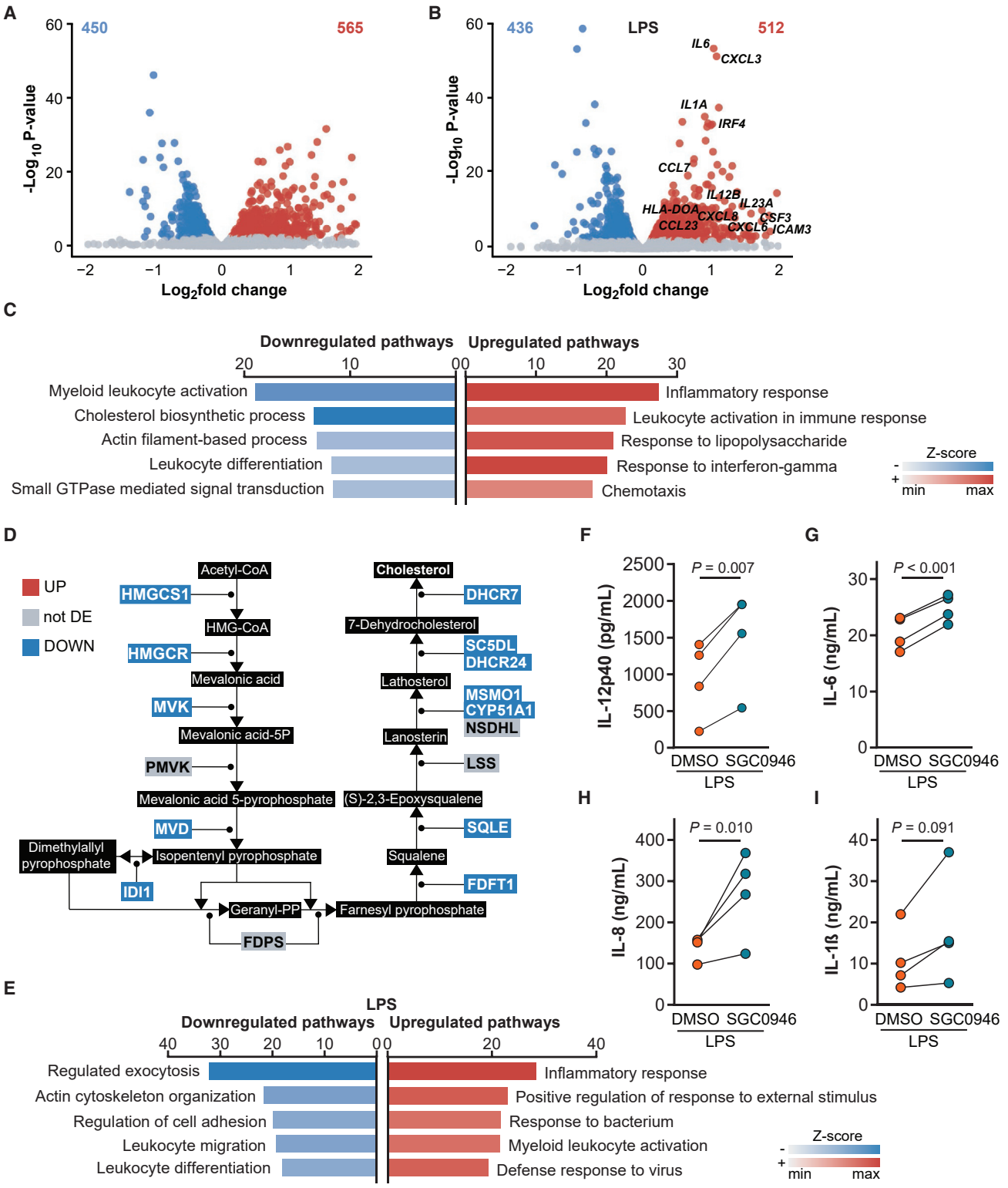

(legend on next page)

is flanked by *loxP* sites leading to a frameshift and premature stops upon exon 2 deletion. *Dot1l* mRNA levels were significantly reduced (83.55%) in *Dot1l*-deficient peritoneal macrophages (PMs) and BMDMs (97.38%) compared with WT macrophages, while *Dot1l* expression was unchanged in neutrophils and B cells (Figure 6B). Global H3K79me2 levels were significantly lower in *Dot1l*-deficient BMDMs (Figures 6C and S4A). No differences were observed between WT and KO BMDM and PM yields during macrophage harvest (Figures S4B and S4C). KO BMDMs were further characterized by RNA-seq and flow cytometry. KO BMDMs had a similar phenotype as SGC0946-treated BMDMs and hMDMs, consisting of a suppressed cholesterol biosynthesis pathway and a hyper-activated inflammatory response (Figures S4D–S4K).

Myeloid *Dot1l* deficiency promotes atherosclerotic plaque instability

To study the involvement of macrophage DOT1L in chronic lipid-driven inflammatory disease *in vivo*, we employed a mouse model for atherosclerosis (Figure 6D). Briefly, bone marrow from either WT or KO mice was transplanted into $Ldlr^{-/-}$ mice. After recovery, mice received a high cholesterol diet (HCD) for 9 weeks to induce atherosclerosis. Subsequently, single-cell RNA sequencing (scRNA-seq) was performed on sorted viable $CD45^{+}$ cells of the aortic arch, and the aortic root was used for histological assessment of the disease. KO PMs showed a 68.5% lower *Dot1l* expression compared with WT, which was similar in regular *Dot1l*-deleted animals, indicating efficient bone marrow reconstitution (Figure 6E). Bodyweight and plasma triglyceride, cholesterol, and alanine transaminase levels were not affected by the myeloid *Dot1l* deficiency (Figures S5A–S5D). Blood monocyte and neutrophil percentages were lower in the KO mice, while eosinophil, B cell, and T cell percentages were not altered (Figure 6F). Interestingly, the *Dot1l*-deficient mice had proportionally more circulating pro-inflammatory monocytes ($Ly6C^{hi}$; Figure 6G), indicating a hyperinflammatory state.

Although myeloid *Dot1l* deficiency did not alter atherosclerotic lesion size, necrotic core size was significantly increased (8.7% in WT transplanted mice versus 13.4% in KO transplanted mice, $p < 0.01$) (Figures 6H–6J). Furthermore, while we did not observe any differences in collagen, macrophage, T cell, and B cell content, we found more infiltrated neutrophils within the KO atherosclerotic plaques (Figures 6K–6M and S5E–S5H). Additionally, plasma levels of markers of systemic inflammatory activation including IL-10 and IFN-γ were significantly higher in KO mice with atherosclerosis (Figures 6N and 6O). Taken together, atherosclerotic myeloid *Dot1l*-deficient mice have pro-inflammatory characteristics with enhanced necrotic core formation and neutrophil accumulation, all unfavorable features of atherosclerosis.

Dot1l-deficient inflammatory plaque macrophages are more activated

scRNA-seq analysis of the immune cells ($CD45^{+}$) in the aortic atherosclerotic plaques identified four different macrophage subsets (Figures 7A, S6A, and S6B). Resident-like macrophages were recognized by expression of folate receptor beta (*Folr2*), lymphatic vessel endothelial hyaluronan receptor 1 (*Lyve1*), and coagulation factor XIII A chain (*F13a1*), $Trem2^{hi}$ foamy macrophages by expression of triggering receptor expressed on myeloid cells 2 (*Trem2*) and *Cd72*, $Trem2^{lo}$ foamy macrophages by expression of fatty acid binding protein 4 (*Fabp4*), arachidonate 15-lipoxygenase (*Alox15*) combined with low *Trem2*, and inflammatory macrophages by the expression of CCAAT enhancer binding protein beta (*Cebpb*), *Il1b*, and *Cxcr4* (Figure 7B). No population size differences were observed between WT and KO of each macrophage subset (Figure S6C). Pathway analysis of the differentially expressed genes ($p < 0.05$) between WT and KO revealed that among all macrophage subsets, inflammatory response-related pathways were altered, with the highest significance in the inflammatory macrophage subset (Figures 7C and S6D). Other enriched pathways include the apoptotic signaling pathway in the $Trem2^{lo}$ foamy macrophages and positive regulation of endocytosis in the $Trem2^{hi}$ foamy macrophages. Specifically, the "Response to IFN-β/γ" and "Defense response to other organisms" pathways are altered in inflammatory plaque macrophages of the KO mice. Among the differentially expressed genes of the inflammatory macrophages were key interferon-regulated genes such as *Fcgr1*, *Ifi204*, *Ifi205*, *Isg15*, *Ifi27l2a*, and *Irf7*. All of these were significantly upregulated in the KO inflammatory plaque macrophages ($p < 0.001$, Figure 7D). To conclude, in the inflammatory setting of atherosclerotic disease, *Dot1l* deficiency leads to a more activated phenotype of plaque macrophages.

DISCUSSION

Macrophage development and function are controlled by transcriptional and epigenetic processes.[5,26] Previous studies have shown that DOT1L controls T and B cell differentiation and responses.[17–20] Here we show that DOT1L is a central regulator of lipid metabolism and inflammatory responses in

Figure 5. DOT1L suppression results in inhibition of cholesterol synthesis and induction of hyperinflammatory state in human macrophages

(A) Volcano plot of RNA-seq data showing the $\log_2$FC and $-\log_{10}$(p value) of SGC0946/DMSO-treated hMDMs with downregulated genes in blue and upregulated genes in red (FDR < 0.05).

(B) Volcano plot of RNA-seq data after TLR4 activation with 3 h of LPS showing the $\log_2$FC and $-\log_{10}$(p value) of SGC0946/DMSO-treated hMDMs with downregulated genes in blue and upregulated genes in red (FDR < 0.05). Numerous pro-inflammatory transcripts are labeled.

(C) Top five downregulated and upregulated pathways of the Gene Ontology pathway analysis of differentially expressed genes (FDR < 0.05) between SGC0946- and DMSO-treated hMDMs.

(D) Gene expression changes of the enzymes regulating the cholesterol biosynthesis pathway after SGC0946 treatment in hMDMs.

(E) Top five downregulated and upregulated pathways of the Gene Ontology pathway analysis of differentially expressed genes (FDR < 0.05) of SGC0946/DMSO-treated hMDMs after 3 h of LPS stimulation.

(F–I) After 24 h of LPS exposure, DMSO- and SGC0946-treated hMDM cytokine secretion of (F) IL-12p40, (G) IL-6, (H) IL-8, and (I) IL-1β was determined. (A–I) n = 4 biological replicates per group. (F and G) p values were calculated using a two-tailed paired t test.

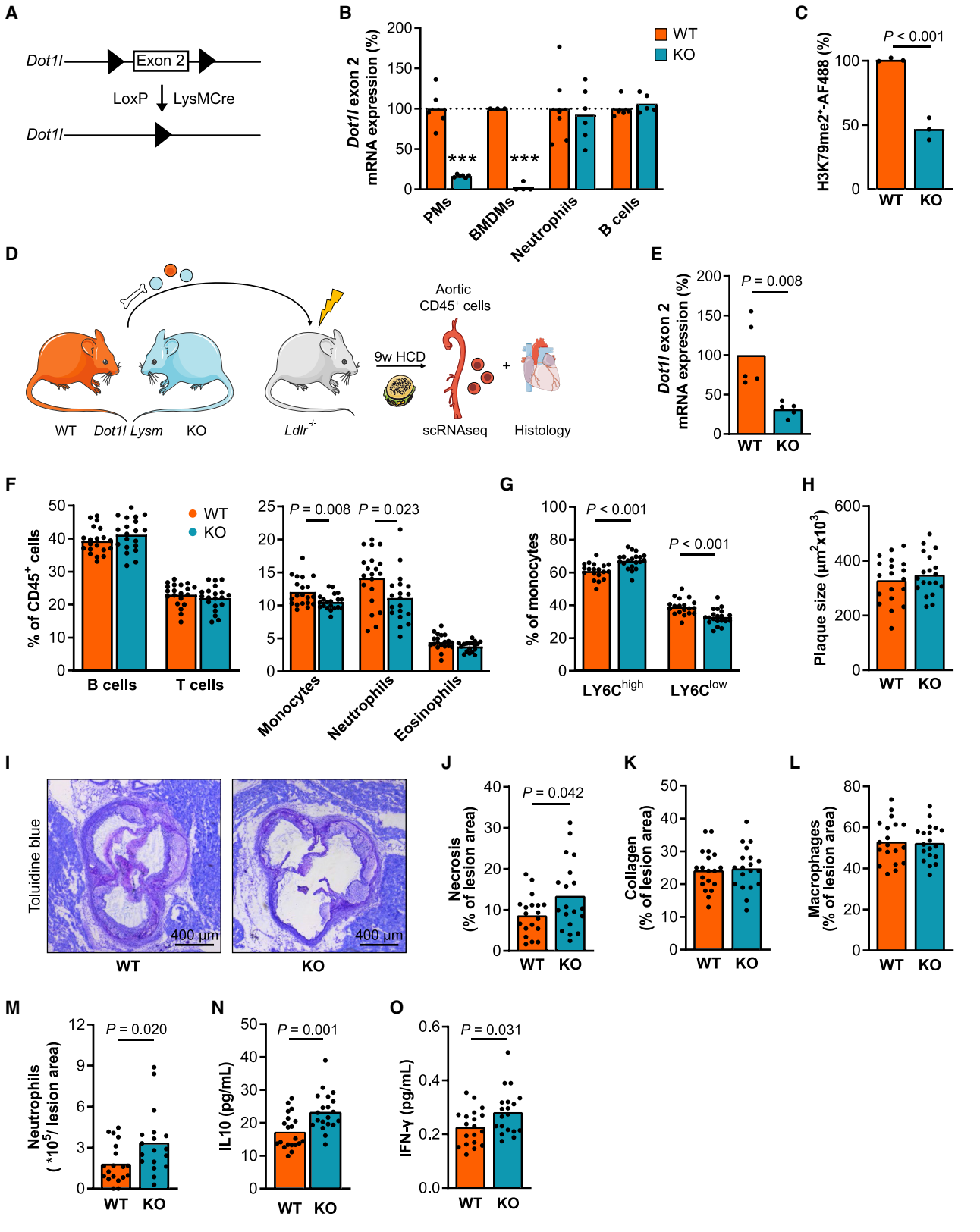

(legend on next page)

macrophages (graphical abstract). DOT1L inhibition results in hyperinflammatory macrophages with defective cholesterol and fatty acid synthesis gene programs. DOT1L-mediated H3K79 histone methylation is associated with gene transcription[13] and is present on genes that are involved in the synthesis of cholesterol and fatty acids, including master regulators *Srebf1* and *Srebf2*. Consequently, suppressed cholesterol and fatty acids pathways program a hyperinflammatory state in macrophages particularly characterized by enhanced IFN signaling. *In vivo*, we confirm that myeloid *Dot1l* deficiency affects chronic inflammatory disease by increasing the activation of inflammatory plaque macrophages and leads to an unstable, exacerbated plaque phenotype in a model for atherosclerosis.

At the start of this study, we found that the optimal starting point of DOT1L inhibition with the SGC0946-specific inhibitor was at the onset of differentiation, although inhibition from day 3 resulted in only slightly more H3K79me2 formation. Compared with these longer incubation periods (from the onset and day 3), only 1 day of DOT1L inhibition resulted in much more H3K79me2 formation and is, therefore, less effective. H3K79me2 loss is a slow process that requires dilution by proliferation-dependent and proliferation-independent histone exchange.[27] Thus ideally, SGC0946 should be applied when bone marrow cells are still dividing.

As H3K79me2/3 modifications are associated with gene transcription,[11–13] we hypothesized that the genes and associated pathways that are most active in macrophages would be targeted by DOT1L inhibition. We confirmed this by showing that genes that are downregulated by DOT1L inhibition had higher basal gene expression levels and contained high H3K79me2 levels compared with genes that were upregulated or not affected by DOT1L inhibition. Pathway analysis on these downregulated genes revealed that these play a role in lipid biosynthetic pathways that are critical for the regulation of many macrophage functions. However, the results also showed that not all genes require DOT1L/H3K79me for gene expression, which has been observed before.[28,29] Why some genes depend on H3K79 methylation and others do not is yet unknown. Notably, Godfrey and colleagues showed that some genes contain a 3′ enhancer located in H3K79me2/3 marked regions that can make them more prone to DOT1L regulation.[28]

While other researchers found a reduced production of IL6 and IFN-β upon *Dot1l* silencing using siRNAs in THP-1 cells,[30] we found increased production of IFN-β by BMDMs and IL6 by hMDMs upon DOT1L inhibition using SGC0946. The distinct developmental origins and phenotypic characteristics of PMA-differentiated THP-1 cells in combination with the different methods of DOT1L inhibition might explain these contradictory results.[31]

We found that DOT1L directly regulates cholesterol and fatty acids synthesis pathways in macrophages. Although not as strong as the effect we observed in macrophages, DOT1L was also found to affect lipid metabolism in human ovarian cancer cells[32] and mouse cerebellar granule cells.[33] Cellular metabolism, including lipid metabolism, greatly affects macrophage function.[34] SREBP1 and SREBP2 are the master transcriptional regulators of fatty acid and cholesterol synthesis, respectively.[22] We showed that almost half of the genes that were downregulated by DOT1L inhibition are also directly regulated by SREBP1. Previous work has shown that blockade of SREBP1 and SREBP2 leads to hyperinflammatory macrophages.[25,35] Oishi et al. demonstrated that *Srebf1*$^{-/-}$ BMDMs have a suppressed production of anti-inflammatory polyunsaturated fatty acids resulting in incomplete resolution of TLR4 activation.[35] Furthermore, SREBP1 was identified as the most upregulated transcription factor in anti-inflammatory compared with pro-inflammatory (IL-4 versus LPS-stimulated) macrophages.[36] Moreover, York et al. found that limiting cholesterol synthesis enhances specifically type I IFN signaling in THP-1 cells.[25] Our data show that DOT1L-mediated suppression of SREBPs also leads to a hyperactivated phenotype displaying an enriched IFN signature. Interestingly, *Srebf2* was also identified as a candidate negative transcriptional regulator affected by DOT1L in T cells.[17] Thus, the hyperinflammatory responses of DOT1L-inhibited and *Dot1l*-deficient macrophages are very likely the result of suppressed SREBP1 and SREBP2 pathways.

We used an LXR agonist (GW3965) to test whether *Srebf1* induction is blocked by SGC0946 treatment in macrophages. Indeed, GW3965 induced the transcription of a subset of genes of the lipid metabolism pathway that are downregulated after DOT1L inhibition. Combined treatment of GW3965 with SGC0946—while still upregulating these genes in absolute terms—preserved the inhibitory effect of SGC0946. Apart from the fact that H3K79me2 levels positively correlate with

Figure 6. Myeloid *Dot1l*-deficiency promotes atherosclerotic plaque instability

(A) Myeloid-specific *Dot1l* KO mice were bred by crossing mice bearing lox-P-targeted *Dot1l* (exon 2) with mice carrying the lysozyme-M Cre (*LysMcre*) recombinase transgene.

(B) *Dot1l* exon 2 mRNA expression in WT and KO thioglycollate-elicited PMs, BMDMs, bone marrow neutrophils, and splenic B cells. n = 3–6 biological replicates per group. ***$p < 0.0001$.

(C) Percentage H3K79me2-positive subset of WT and KO BMDMs determined by flow cytometry. n = 3 biological replicates per group.

(D) Schematic illustration of the experimental setup of the atherosclerosis mouse model (adapted from Servier Medical Art).

(E) *Dot1l* mRNA expression of PMs after 9 weeks of HCD. n = 5 biological replicates per group.

(F) Percentage of blood immune cell subsets assessed by flow cytometry after 9 weeks of HCD.

(G) Percentage of LY6C^{high} and LY6C^{low} blood monocyte subsets assessed by flow cytometry after 9 weeks of HCD.

(H) Quantification of plaque size after 9 weeks of HCD. One data point represents the sum of the plaque size of the three valves per mouse.

(I) Representative toluidine blue staining of the aortic roots after 9 weeks of HCD.

(J–L) Necrotic core percentage (J), collagen percentage (K), and macrophage percentages (L) (MOMA-2 staining) of total lesion area after 9 weeks of HCD.

(M–O) Neutrophil (Ly6G) count (M), Plasma IL-10 (N), and IFN-γ levels (O) of *Dot1l* WT and KO mice fed an HCD for 9 weeks. (F–O) n = 20 biological replicates per group. (B–O) p values were calculated using multiple two-tailed unpaired t-tests.

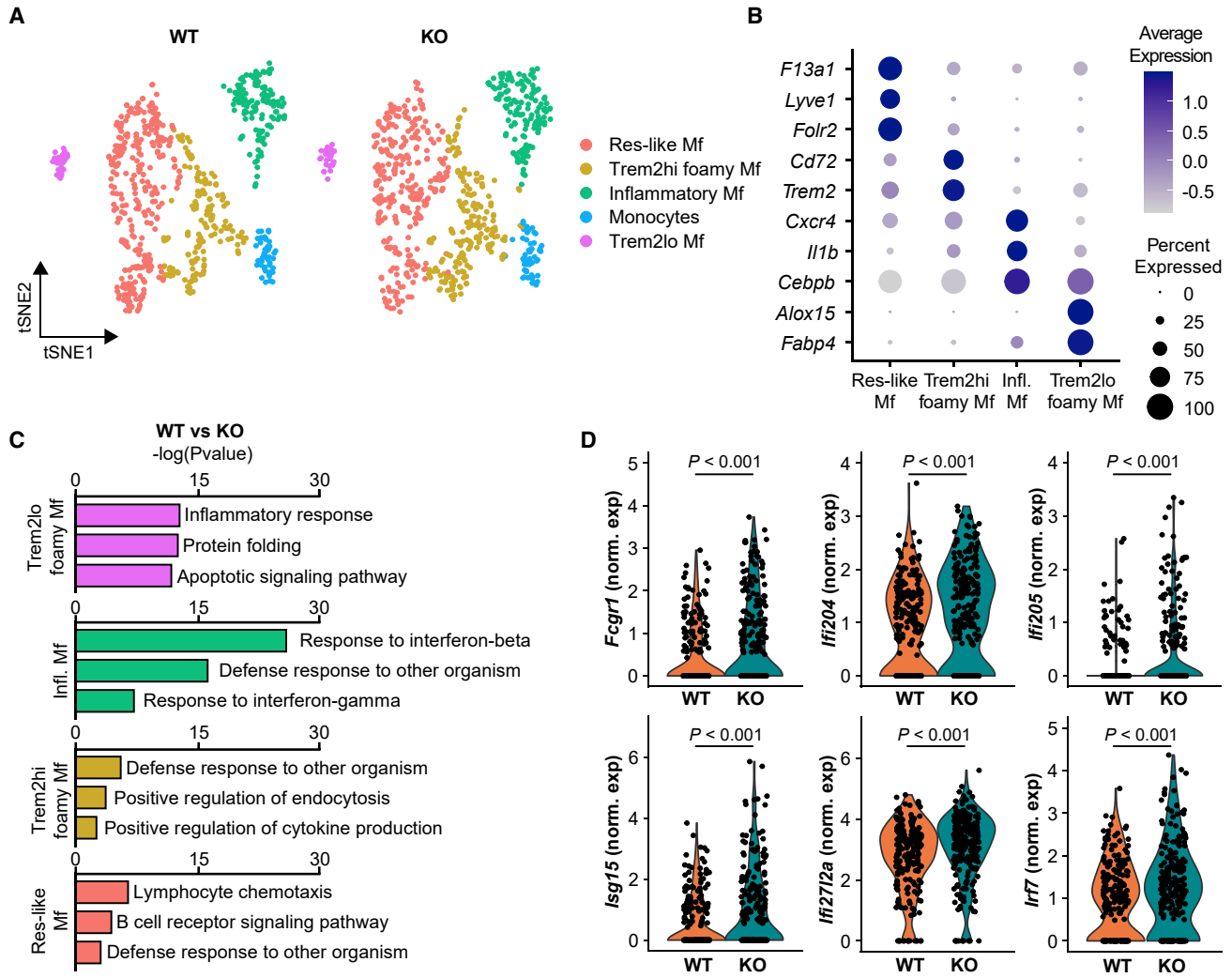

Figure 7. *Dot1l* KO inflammatory plaque macrophages are more activated

(A) Annotated tSNE visualizations of the identified monocyte and macrophage subsets of scRNA-seq data of viable CD45$^+$ cells of the atherosclerotic aortic arch of myeloid *Dot1l* WT and KO mice.

(B) Macrophage subsets were annotated via cluster marker identification and expression levels (differentially expressed genes) for each of the macrophage clusters and confirmed by literature.

(C) Top three pathways of the Gene Ontology pathway analysis of differentially expressed genes ($p < 0.05$) between WT and KO plaque macrophages per macrophage subset.

(D) The normalized expression of numerous interferon-related genes was significantly increased in *Dot1l* KO inflammatory plaque macrophages compared to WT.

(A–D) cells of n = 3–10 aortas per group were pooled to create two pools per genotype.

transcription,[13] activating transcription factors can induce gene expression irrespective of H3K79me2 levels.

Since DOT1L inhibition results in hyperinflammatory macrophages, we assessed whether DOT1L also affects chronic inflammatory diseases like atherosclerosis. We found that myeloid *Dot1l* deficiency *in vivo* results in unstable atherosclerotic plaques consisting of more necrosis, more infiltrating neutrophils, proportionally more circulating pro-inflammatory monocytes, and increased levels of plasma IFN-γ and IL-10. These are fundamental characteristics of vulnerable, unstable plaques.[37–40] Plaque vulnerability depends on plaque composition rather than plaque volume,[41] and characteristics like necrotic lipid-rich core formation and inflammatory profile of the lesions highly contribute to potential clinical complications in patients.[42] Although IL-10 has been described as an anti-inflammatory cytokine, increased IL-10 levels have been reported in unstable plaques,[43] and plasma IL-10 levels are associated with adverse outcomes in acute coronary syndrome.[44] Applying scRNA-seq, we confirmed that inflammatory plaque macrophages were more activated and displayed an enriched IFN signature, a similar phenotype as we observed *in vitro*. Moreover, previous work has shown that myeloid type I IFN signaling is upregulated in ruptured human atherosclerotic plaques and is associated with necrotic core formation and neutrophil infiltration.[45]

IFN-driven macrophage activation may contribute to plaque instability by promoting local inflammation including recruitment of immune cells, enhanced matrix production, and a tissue damage and impaired wound healing phenotype.[3,46] The IFN signature of myeloid *Dot1l* KO inflammatory plaque macrophages phenocopies the more activated state displayed *in vitro* by DOT1L-inhibited human and mouse macrophages. This more inflammatory macrophage state may have contributed to the unstable, exacerbated plaque phenotype of the *Dot1l*-deficient mice. To conclude, *Dot1l* deficiency results in an unfavorable prognosis for atherosclerotic mice. Since the phenotype of mouse and human DOT1L-inhibited macrophages is similar, myeloid DOT1L possibly plays a protective role in human atherosclerosis as well.

Apart from the oncology field, epigenome-influencing strategies to treat disease remain poorly investigated. More knowledge about the molecular players of epigenetics and the discovery of target-directed applications may stimulate the development of therapeutic approaches for immune system disorders.[47] Given that DOT1L plays a crucial role in the immune system at different levels, clinical trials, such as using pinometostat (EPZ-5676) for the treatment of leukemia, and future research should focus and be aware of potential immunological effects of inhibiting DOT1L. We have here demonstrated an essential role for DOT1L and H3K79 methylation in macrophage physiology and linked this to atherosclerotic disease *in vivo*. Our data also suggest that targeting myeloid DOT1L may be beneficial in settings where enhancing inflammatory responses is required.

Limitations of the study

Our data suggest a pathway where inhibition of DOT1L activity leads to suppressed SREBP lipid synthetic pathways that consequently enhance macrophage inflammatory activation. The limitations of our study are the following. (1) We do not rule out the possibility that also other pathways (other than lipid-related) can be involved in the induction of the hyperinflammatory macrophage phenotype. Additional experiments, such as in which SREBPs are overexpressed, are essential to further confirm the link between DOT1L, these pathways, and hyperinflammatory macrophage phenotype. (2) Supplementary studies involving lipid uptake, synthesis, and secretion identification and quantifications are necessary to determine the biological impact of the suppressed lipid synthetic gene programs. (3) The detection of nuclear SREBP2 protein was only performed on a pool of three DMSO- and three SGC0946-treated BMDMs. (4) We could not corroborate the macrophage lipid phenotype in atherosclerotic lesions in mice, possibly because of the hyperlipidemic background of the mouse model.

STAR★METHODS

Detailed methods are provided in the online version of this paper and include the following:

SUPPLEMENTAL INFORMATION

Supplemental information can be found online at https://doi.org/10.1016/j.celrep.2022.111703.

ACKNOWLEDGMENTS

This work was supported by the Netherlands Heart Foundation (CVON 2011/B019, CVON 2017-20), the Netherlands Heart Foundation and Spark-Holding BV (2015B002, 2019B016), the European Union (ITN grant EPIMAC), Leducq Foundation (LEAN Transatlantic Network Grant), AMC Fellowship, Amsterdam UMC, Dutch Cancer Society (NKI2018-1/11490 and NKI2019-2/12825), ZonMw (ZonMW Top91218022, Open competition 09120011910025), and a Vici grant from the Netherlands Organization for Scientific Research (NWO; 016.176.643).

AUTHOR CONTRIBUTIONS

L.W., K.H.M.P., A.E.N., H.J., F.L., and M.P.J.W. designed the research or gave critical input to the design. L.W. performed the majority of experiments with contributions from K.H.M.P. (H3K79me2 ChIP-seq), C.P.A.A.R. (bone marrow isolation and atherosclerosis mouse model), H.C. (human monocyte isolation), G.R.G. (sequencing library preparation), R.S., A.G., S.W., and N.Z. (PF-429242 2HCl experiments), N.J.S. (SREBP1/2 ChIP-seq), and M.G., A.E.N., M.T., and L.A.B. (atherosclerosis mouse model). L.W. analyzed the data and generated a graphical representation. L.W. wrote the manuscript, and M.P.J.W., F.L., N.Z., H.J., K.H.M.P., A.E.N., M.G., L.A.B., and H.C. gave critical feedback. M.P.J.W. initiated and supervised the study.

DECLARATION OF INTERESTS

The authors declare no competing interests.

Received: November 16, 2021
Revised: August 29, 2022
Accepted: November 1, 2022
Published: November 22, 2022

REFERENCES

1. Wynn, T.A., Chawla, A., and Pollard, J.W. (2013). Macrophage biology in development, homeostasis and disease. Nature *496*, 445–455. https://doi.org/10.1038/nature12034.

2. Roth, G.A., Abate, D., Abate, K.H., Abay, S.M., Abbafati, C., Abbasi, N., Abbastabar, H., Abd-Allah, F., Abdela, J., Abdelalim, A., et al. (2018). Global, regional, and national age-sex-specific mortality for 282 causes of death in 195 countries and territories, 1980–2017: a systematic analysis for the Global Burden of Disease Study 2017. Lancet *392*, 1736–1788. https://doi.org/10.1016/S0140-6736(18)32203-7.

3. Willemsen, L., and de Winther, M.P.J. (2020). Macrophage subsets in atherosclerosis as defined by single-cell technologies. J. Pathol. *250*, 705–714. https://doi.org/10.1002/path.5392.

4. Moore, K.J., Sheedy, F.J., and Fisher, E.A. (2013). Macrophages in atherosclerosis: a dynamic balance. Nat. Rev. Immunol. *13*, 709–721. https://doi.org/10.1038/nri3520.

5. Hoeksema, M. a, and de Winther, M.P. (2016). Epigenetic regulation of monocyte and macrophage function. Antioxid Redox Signal *25*, 758–774. https://doi.org/10.1089/ars.2016.6695.

6. Kuznetsova, T., Prange, K.H.M., Glass, C.K., and de Winther, M.P.J. (2020). Transcriptional and epigenetic regulation of macrophages in atherosclerosis. Nat. Rev. Cardiol. *17*, 216–228. https://doi.org/10.1038/s41569-019-0265-3.

7. Arrowsmith, C.H., Bountra, C., Fish, P.V., Lee, K., and Schapira, M. (2012). Epigenetic protein families: a new frontier for drug discovery. Nat. Rev. Drug Discov. *11*, 384–400. https://doi.org/10.1038/nrd3674.

8. Neele, A.E., Willemsen, L., Chen, H.J., Dzobo, K.E., and de Winther, M.P.J. (2020). Targeting epigenetics as atherosclerosis treatment: an updated view. Curr. Opin. Lipidol. *31*, 324–330. https://doi.org/10.1097/MOL.0000000000000711.

9. Van den Bossche, J., Neele, A.E., Hoeksema, M.A., and de Winther, M.P.J. (2014). Macrophage polarization: the epigenetic point of view. Curr. Opin. Lipidol. *25*, 367–373. https://doi.org/10.1097/MOL.0000000000000109.

10. Feng, Q., Wang, H., Ng, H.H., Erdjument-Bromage, H., Tempst, P., Struhl, K., and Zhang, Y. (2002). Methylation of H3-lysine 79 is mediated by a new family of HMTases without a SET domain. Curr. Biol. *12*, 1052–1058. https://doi.org/10.1016/s0960-9822(02)00901-6.

11. Vlaming, H., and van Leeuwen, F. (2016). The upstreams and downstreams of H3K79 methylation by DOT1L. Chromosoma *125*, 593–605. https://doi.org/10.1007/s00412-015-0570-5.

12. Wood, K., Tellier, M., and Murphy, S. (2018). DOT1L and H3K79 methylation in transcription and genomic stability. Biomolecules *8*, 1–16. https://doi.org/10.3390/biom8010011.

13. Steger, D.J., Lefterova, M.I., Ying, L., Stonestrom, A.J., Schupp, M., Zhuo, D., Vakoc, A.L., Kim, J.-E., Chen, J., Lazar, M.A., et al. (2008). DOT1L/KMT4 recruitment and H3K79 methylation are ubiquitously coupled with gene transcription in mammalian cells. Mol. Cell Biol. *28*, 2825–2839. https://doi.org/10.1128/MCB.02076-07.

14. McLean, C.M., Karemaker, I.D., and van Leeuwen, F. (2014). The emerging roles of DOT1L in leukemia and normal development. Leukemia *28*, 1–8. https://doi.org/10.1038/leu.2014.169.

15. Stein, E.M., Garcia-Manero, G., Rizzieri, D.A., Tibes, R., Berdeja, J.G., Jongen-Lavrencic, M., Altman, J.K., Dohner, H., Thomson, B., Blakemore, S.J., et al. (2015). A phase 1 study of the DOT1L inhibitor, Pinometostat (EPZ-5676), in adults with relapsed or refractory leukemia: safety, clinical activity, exposure and target inhibition. Blood *126*, 2547. https://doi.org/10.1182/blood.V126.23.2547.2547.

16. Shukla, N., Wetmore, C., O'Brien, M.M., Silverman, L.B., Brown, P., Cooper, T.M., Thomson, B., Blakemore, S.J., Daigle, S., Suttle, B., et al. (2016). Final report of phase 1 study of the DOT1L inhibitor, Pinometostat (EPZ-5676), in children with relapsed or refractory MLL-r acute leukemia. Blood *128*, 2780. https://doi.org/10.1182/blood.V128.22.2780.2780.

17. Kwesi-Maliepaard, E.M., Aslam, M.A., Alemdehy, M.F., Van Den Brand, T.V., McLean, C., Vlaming, H., van Welsem, T., Korthout, T., Lancini, C., Hendriks, S., et al. (2020). The histone methyltransferase DOT1L prevents antigen-independent differentiation and safeguards epigenetic identity of CD8+ T cells. Proc. Natl. Acad. Sci. USA *117*, 20706–20716. https://doi.org/10.1073/pnas.1920372117.

18. Aslam, M.A., Alemdehy, M.F., Kwesi-Maliepaard, E.M., Caganova, M., Pardieck, I.N., van den Brand, T., Muhaimin, F.I., van Welsem, T., de Rink, I., Song, J.Y., et al. (2021). Histone methyltransferase DOT1L controls state-specific identity during B cell differentiation. EMBO Rep. *22*. https://doi.org/10.1101/826370.

19. Kealy, L., Di Pietro, A., Hailes, L., Scheer, S., Dalit, L., Groom, J.R., Zaph, C., and Good-Jacobson, K.L. (2020). The histone methyltransferase DOT1L is essential for humoral immune responses. Cell Rep. *33*, 108504. https://doi.org/10.1016/j.celrep.2020.108504.

20. Scheer, S., Runting, J., Bramhall, M., Russ, B., Zaini, A., Ellemor, J., Rodrigues, G., Ng, J., and Zaph, C. (2020). The methyltransferase DOT1L controls activation and lineage integrity in CD4+ T cells during infection and inflammation. Cell Rep. *33*, 108505. https://doi.org/10.1016/j.celrep.2020.108505.

21. Yu, W., Chory, E.J., Wernimont, A.K., Tempel, W., Scopton, A., Federation, A., Marineau, J.J., Qi, J., Barsyte-Lovejoy, D., Yi, J., et al. (2012). Catalytic site remodelling of the DOT1L methyltransferase by selective inhibitors. Nat. Commun. *3*, 1–12. https://doi.org/10.1038/ncomms2304.

22. DeBose-Boyd, R.A., and Ye, J. (2018). SREBPs in lipid metabolism, insulin signaling, and beyond. Trends Biochem. Sci. *43*, 358–368. https://doi.org/10.1016/j.tibs.2018.01.005.

23. Xiong, S., Chirala, S.S., and Wakil, S.J. (2000). Sterol regulation of human fatty acid synthase promoter I requires nuclear factor-Y- and Sp-1-binding sites. Proc. Natl. Acad. Sci. USA *97*, 3948–3953. https://doi.org/10.1073/pnas.040574197.

24. Yoshikawa, T., Shimano, H., Amemiya-Kudo, M., Yahagi, N., Hasty, A.H., Matsuzaka, T., Okazaki, H., Tamura, Y., Iizuka, Y., Ohashi, K., et al. (2001). Identification of liver X receptor-retinoid X receptor as an activator of the sterol regulatory element-binding protein 1c gene promoter. Mol. Cell Biol. *21*, 2991–3000. https://doi.org/10.1128/MCB.21.9.2991-3000.2001.

25. York, A.G., Williams, K.J., Argus, J.P., Zhou, Q.D., Brar, G., Vergnes, L., Gray, E.E., Zhen, A., Wu, N.C., Yamada, D.H., et al. (2015). Limiting cholesterol biosynthetic flux spontaneously engages type i IFN signaling. Cell *163*, 1716–1729. https://doi.org/10.1016/j.cell.2015.11.045.

26. Chen, S., Yang, J., Wei, Y., and Wei, X. (2020). Epigenetic regulation of macrophages: from homeostasis maintenance to host defense. Cell. Mol. Immunol. *17*, 36–49. https://doi.org/10.1038/s41423-019-0315-0.

27. De Vos, D., Frederiks, F., Terweij, M., Van Welsem, T., Verzijlbergen, K.F., Iachina, E., De Graaf, E.L., Maarten Altelaar, A.F., Oudgenoeg, G., Heck, A.J.R., et al. (2011). Progressive methylation of ageing histones by Dot1 functions as a timer. EMBO Rep. *12*, 956–962. https://doi.org/10.1038/embor.2011.131.

28. Godfrey, L., Crump, N.T., Thorne, R., Lau, I.J., Repapi, E., Dimou, D., Smith, A.L., Harman, J.R., Telenius, J.M., Oudelaar, A.M., et al. (2019). DOT1L inhibition reveals a distinct subset of enhancers dependent on H3K79 methylation. Nat. Commun. *10*, 1–15. https://doi.org/10.1038/s41467-019-10844-3.

29. Kerry, J., Godfrey, L., Repapi, E., Tapia, M., Blackledge, N.P., Ma, H., Ballabio, E., O'Byrne, S., Ponthan, F., Heidenreich, O., et al. (2017). MLL-AF4 spreading identifies binding sites that are distinct from super-enhancers and that govern sensitivity to DOT1L inhibition in leukemia. Cell Rep. *18*, 482–495. https://doi.org/10.1016/j.celrep.2016.12.054.

30. Chen, X., Liu, X., Zhang, Y., Huai, W., Zhou, Q., Xu, S., Chen, X., Li, N., and Cao, X. (2018). Methyltransferase Dot1l preferentially promotes innate IL-6 and IFN-β production by mediating H3K79me2/3 methylation in macrophages. Cell. Mol. Immunol. *17*, 76–84. https://doi.org/10.1038/s41423-018-0170-4.

31. Tedesco, S., De Majo, F., Kim, J., Trenti, A., Trevisi, L., Fadini, G.P., Bolego, C., Zandstra, P.W., Cignarella, A., and Vitiello, L. (2018). Convenience versus biological significance: are PMA-differentiated THP-1 cells a reliable substitute for blood-derived macrophages when studying in vitro

polarization? Front. Pharmacol. *9*. https://doi.org/10.3389/fphar.2018.00071.

32. Salvati, A., Gigantino, V., Nassa, G., Giurato, G., Alexandrova, E., Rizzo, F., Tarallo, R., and Weisz, A. (2019). The histone methyltransferase dot1l is a functional component of estrogen receptor alpha signaling in ovarian cancer cells. Cancers *11*, 1–18. https://doi.org/10.3390/cancers11111720.
33. Bovio, P.P., Franz, H., Heidrich, S., Rauleac, T., Kilpert, F., Manke, T., and Vogel, T. (2019). Differential methylation of H3K79 reveals DOT1L target genes and function in the cerebellum in vivo. Mol. Neurobiol. *56*, 4273–4287. https://doi.org/10.1007/s12035-018-1377-1.
34. Yan, J., and Horng, T. (2020). Lipid metabolism in regulation of macrophage functions. Trends Cell Biol. *30*, 979–989. https://doi.org/10.1016/j.tcb.2020.09.006.
35. Oishi, Y., Spann, N.J., Link, V.M., Muse, E.D., Strid, T., Edillor, C., Kolar, M.J., Matsuzaka, T., Hayakawa, S., Tao, J., et al. (2017). SREBP1 contributes to resolution of pro-inflammatory TLR4 signaling by reprogramming fatty acid metabolism. Cell Metab *25*, 412–427. https://doi.org/10.1016/j.cmet.2016.11.009.
36. Bidault, G., Virtue, S., Petkevicius, K., Jolin, H.E., Dugourd, A., Guénantin, A.C., Leggat, J., Mahler-Araujo, B., Lam, B.Y.H., Ma, M.K., et al. (2021). SREBP1-induced fatty acid synthesis depletes macrophages antioxidant defences to promote their alternative activation. Nat Metab *3*, 1150–1162. https://doi.org/10.1038/s42255-021-00440-5.
37. Ionita, M.G., van den Borne, P., Catanzariti, L.M., Moll, F.L., de Vries, J.-P.P.M., Pasterkamp, G., Vink, A., and de Kleijn, D.P.V. (2010). High neutrophil numbers in human carotid atherosclerotic plaques are associated with characteristics of rupture-prone lesions. Arterioscler. Thromb. Vasc. Biol. *30*, 1842–1848. https://doi.org/10.1161/ATVBAHA.110.209296.
38. Finn, A.V., Nakano, M., Narula, J., Kolodgie, F.D., and Virmani, R. (2010). Concept of vulnerable/unstable plaque. Arterioscler. Thromb. Vasc. Biol. *30*, 1282–1292. https://doi.org/10.1161/ATVBAHA.108.179739.
39. Swirski, F.K., Libby, P., Aikawa, E., Alcaide, P., Luscinskas, F.W., Weissleder, R., and Pittet, M.J. (2007). Ly-6Chi monocytes dominate hypercholesterolemia-associated monocytosis and give rise to macrophages in atheromata. J. Clin. Invest. *117*, 195–205. https://doi.org/10.1172/JCI29950.
40. Moss, J.W.E., and Ramji, D.P. (2015). Interferon-γ: promising therapeutic target in atherosclerosis. World J. Exp. Med. *5*, 154–160. https://doi.org/10.5493/wjem.v5.i3.154.
41. Bentzon, J.F., Otsuka, F., Virmani, R., and Falk, E. (2014). Mechanisms of plaque formation and rupture. Circ. Res. *114*, 1852–1866. https://doi.org/10.1161/CIRCRESAHA.114.302721.
42. Libby, P., Pasterkamp, G., Crea, F., and Jang, I.K. (2019). Reassessing the mechanisms of acute coronary syndromes: the "vulnerable plaque" and superficial erosion. Circ. Res. *124*, 150–160. https://doi.org/10.1161/CIRCRESAHA.118.311098.
43. Nishihira, K., Imamura, T., Yamashita, A., Hatakeyama, K., Shibata, Y., Nagatomo, Y., Date, H., Kita, T., Eto, T., and Asada, Y. (2006). Increased expression of interleukin-10 in unstable plaque obtained by directional coronary atherectomy. Eur. Heart J. *27*, 1685–1689. https://doi.org/10.1093/eurheartj/ehl058.
44. Cavusoglu, E., Marmur, J.D., Hojjati, M.R., Chopra, V., Butala, M., Subnani, R., Huda, M.S., Yanamadala, S., Ruwende, C., Eng, C., et al. (2011). Plasma interleukin-10 levels and adverse outcomes in acute coronary syndrome. Am. J. Med. *124*, 724–730. https://doi.org/10.1016/j.amjmed.2011.02.040.
45. Goossens, P., Gijbels, M.J.J., Zernecke, A., Eijgelaar, W., Vergouwe, M.N., van der Made, I., Vanderlocht, J., Beckers, L., Buurman, W.A., Daemen, M.J.A.P., et al. (2010). Myeloid type I interferon signaling promotes atherosclerosis by stimulating macrophage recruitment to lesions. Cell Metab *12*, 142–153. https://doi.org/10.1016/j.cmet.2010.06.008.
46. Chen, H.J., Tas, S.W., and de Winther, M.P.J. (2020). Type-I interferons in atherosclerosis. J. Exp. Med. *217*, 1–24. https://doi.org/10.1084/jem.20190459.
47. Surace, A.E.A., and Hedrich, C.M. (2019). The role of epigenetics in autoimmune/inflammatory disease. Front. Immunol. *10*, 1–16. https://doi.org/10.3389/fimmu.2019.01525.
48. Skarnes, W.C., Rosen, B., West, A.P., Koutsourakis, M., Bushell, W., Iyer, V., Mujica, A.O., Thomas, M., Harrow, J., Cox, T., et al. (2011). A conditional knockout resource for the genome-wide study of mouse gene function. Nature *474*, 337–344. https://doi.org/10.1038/nature10163.
49. Mandoli, A., Prange, K., and Martens, J.H.A. (2014). Genome-wide binding of transcription factors in inv(16) acute myeloid leukemia. Genom Data *2*, 170–172. https://doi.org/10.1016/j.gdata.2014.06.014.
50. Dobin, A., Davis, C.A., Schlesinger, F., Drenkow, J., Zaleski, C., Jha, S., Batut, P., Chaisson, M., and Gingeras, T.R. (2013). STAR: ultrafast universal RNA-seq aligner. Bioinformatics *29*, 15–21. https://doi.org/10.1093/bioinformatics/bts635.
51. Li, H., Handsaker, B., Wysoker, A., Fennell, T., Ruan, J., Homer, N., Marth, G., Abecasis, G., and Durbin, R. (2009). The sequence alignment/map format and SAMtools. Bioinformatics *25*, 2078–2079. https://doi.org/10.1093/bioinformatics/btp352.
52. Heinz, S., Benner, C., Spann, N., Bertolino, E., Lin, Y.C., Laslo, P., Cheng, J.X., Murre, C., Singh, H., and Glass, C.K. (2010). Simple combinations of lineage-determining transcription factors prime cis-regulatory elements required for macrophage and B cell identities. Mol Cell *38*, 576–589. https://doi.org/10.1016/j.molcel.2010.05.004.
53. Love, M.I., Huber, W., and Anders, S. (2014). Moderated estimation of fold change and dispersion for RNA-seq data with DESeq2. Genome Biol. *15*, 1–21. https://doi.org/10.1186/s13059-014-0550-8.
54. Zhou, Y., Zhou, B., Pache, L., Chang, M., Khodabakhshi, A.H., Tanaseichuk, O., Benner, C., and Chanda, S.K. (2019). Metascape provides a biologist-oriented resource for the analysis of systems-level datasets. Nat. Commun. *10*. https://doi.org/10.1038/s41467-019-09234-6.
55. Quinlan, A.R., and Hall, I.M. (2010). BEDTools: a flexible suite of utilities for comparing genomic features. Bioinformatics *26*, 841–842. https://doi.org/10.1093/bioinformatics/btq033.
56. Yu, G., Wang, L.-G., and He, Q.-Y. (2015). ChIPseeker: an R/Bioconductor package for ChIP peak annotation, comparison and visualization. Bioinformatics *31*, 2382–2383. https://doi.org/10.1093/bioinformatics/btv145.
57. Langmead, B., and Salzberg, S.L. (2012). Fast gapped-read alignment with Bowtie 2. Nat. Methods *9*, 357–359. https://doi.org/10.1038/nmeth.1923.
58. Satija, R., Farrell, J.A., Gennert, D., Schier, A.F., and Regev, A. (2015). Spatial reconstruction of single-cell gene expression data. Nat. Biotechnol. *33*, 495–502. https://doi.org/10.1038/nbt.3192.

STAR★METHODS

KEY RESOURCES TABLE

REAGENT or RESOURCE	SOURCE	IDENTIFIER
Antibodies		
CD45R (B220) Monoclonal Antibody (RA3-6B2)	eBioscience	Cat# 14–0452
Rabbit Anti-Rat IgG Antibody, mouse adsorbed (H + L), Biotinylated	Vector Laboratories	Cat# BA-4001; RRID: AB_10015300
CD11b Monoclonal Antibody (M1/70), FITC (FACS)	eBioscience	Cat# 11–0112
PE-Cy™7 Rat Anti-CD11b Clone M1/70 (FACS)	BD Biosciences	Cat# 552850; RRID: AB_394491
CD16/CD32 Monoclonal Antibody 93	eBioscience	Cat# 14–0161; RRID: AB_467133
CD19 Monoclonal Antibody (eBio1D3 (1D3)), PerCP-Cyanine5.5	eBioscience	Cat# 45–0193; RRID: AB_1106999
CD3e Monoclonal Antibody (145-2C11), FITC,	eBioscience	Cat# 11–0031; RRID: AB_464882
CD3 Monoclonal Antibody (KT3)	Bio-Rad	Cat# MCA500G; RRID: AB_321252
CD4 Monoclonal Antibody (GK1.5), APC	eBioscience	Cat# 17–0041; RRID: AB_469320
APC/Cyanine7 anti-mouse CD45 Antibody 30-F11 (FACS)	BioLegend	Cat# 103116; RRID: AB_312981
PE/Cyanine7 anti-mouse CD45 Antibody 30-F11 (Sorting)	BioLegend	Cat# 103114; RRID: AB_312979
PE anti-mouse CD64 (FcγRI) Antibody X54-5/7.1	BioLegend	Cat# 139304; RRID: AB_10612740
CD86 (B7-2) Monoclonal Antibody (GL1), APC	eBioscience	Cat# 17–0862; RRID: AB_469419
CD8a Monoclonal Antibody (53-6.7), PE	eBioscience	Cat# 12–0081; RRID: AB_465530
F4/80 Monoclonal Antibody (BM8), APC-eFluor™ 780	eBioscience	Cat# 47–4801; RRID: AB_2735036
Anti-dimethyl-Histone H3 (Lys79) Antibody, clone NL59, rabbit monoclonal	Sigma	Cat# 04–835
Donkey anti-Rat IgG (H + L) Highly Cross-Adsorbed Secondary Antibody, Alexa Fluor™ 488	ThermoFisher	Cat# A-21208; RRID: AB_2535794
PE Rat Anti-Mouse Ly-6G 1A8 (FACS)	BD Biosciences	Cat# 551461; RRID: AB_394208
Purified Rat Anti-Mouse Ly-6G 1A8 (IHC)	BD Biosciences	Cat# 551459; RRID: AB_394206
Ly-6G/Ly-6C Monoclonal Antibody (RB6-8C5), APC	eBioscience	Cat# 17–5931; RRID: AB_469476
Macrophages/Monocytes antibody MOMA-2	Bio-Rad	Cat# MCA519G; RRID: AB_321970
PerCP/Cyanine5.5 anti-mouse I-A/I-E Antibody M5/114.15.2	BioLegend	Cat# 107626; RRID: AB_2191071
Anti-SREBP-2 Antibody, clone 22D5	Sigma	Cat# MABS1988
Histone H3 (D2B12) XP® Rabbit mAb (ChIP Formulated)	Cell Signaling	Cat# 4620; RRID: AB_1904005
Goat anti-Rabbit IgG (H + L) Poly-HRP Secondary Antibody	Thermofisher	Cat# 32260; RRID: AB_1965959
SREBP-1 Antibody (H-160) (ChIP)	Santa Cruz	Cat# SC-8984; RRID: AB_2194223
SREBP1 Polyclonal Antibody (ChIP)	Thermofisher	Cat# PA1-337; RRID: AB_2194231
Human SREBP2 Antibody (ChIP)	R&D Systems	Cat# AF7119; RRID: AB_10992735

(*Continued on next page*)

Continued

REAGENT or RESOURCE	SOURCE	IDENTIFIER
Biological samples		
Buffy coats	Sanquin Blood Supply	https://www.sanquin.nl/en
Chemicals, peptides, and recombinant proteins		
SGC0946, DOT1L inhibitor	Sigma-Aldrich	SML1107
GW3965, LXR activator	Sigma-Aldrich	G6295
PF-429242 dihydrochloride, S1P inhibitor	Sigma-Aldrich	SML0667
Lipopolysaccharide, *Escherichia coli*; O111:B4	Sigma-Aldrich	L2630
Recombinant murine IFN-γ	PeproTech	315–05
BD Difco™ Dehydrated Culture Media: Fluid Thioglycollate Medium	Thermo Fisher	11,782,834
human M-CSF	Miltenyi Biotec	130-096-492
RPMI 1640 medium	Gibco	52,400
IMDM medium	Gibco	21,056,023
Fetal Bovine Serum	Gibco	10,500,064
Critical commercial assays		
V-PLEX Custom Human Cytokine Proinflammatory Panel 1	MSD	K15049D
ELISA MAX™ Standard Set Human IL-6	BioLegend	430,501
LEGEND MAX™ Human IL-12/IL-23 (p40) ELISA Kit	BioLegend	430,707
Cholesterol CHOD-PAP reagent	Roche Diagnostics	11,489,232
Triglycerides GPO-PAP reagent	Roche Diagnostics	11,488,872
Mouse IFN-beta DuoSet ELISA	R&D Systems	DY8234
ALT Activity Assay	Sigma-Aldrich	MAK052
Deposited data		
Bulk RNA-seq, ChIP-seq, scRNAseq	This paper	GEO: GSE193119
Experimental models: Organisms/strains		
Mouse: C57BL/6J *LysMcre*$^{-}$*Dot1l*$^{fl/fl}$	*LysMcre* crossbreeding was performed in our mice facility	
Mouse: C57BL/6J *LysMcre*$^{+}$*Dot1l*$^{fl/fl}$	*LysMcre* crossbreeding was performed in our mice facility	
Mouse: C57BL/6J *Ldlr*$^{-/-}$	The Jackson Laboratory	JAX:002,207
Oligonucleotides		
Actb, Gapdh, Dot1l, Ppia, Mmp13, Cd86, Ifi44, Ifi205	Sigma-Aldrich	See Table S1
Software and algorithms		
FlowJo software v10.7.0	BD Biosciences	https://www.bdbiosciences.com
Discovery Workbench Software v4.0	MSD	https://www.mesoscale.com
GraphPad Prism v9.1.0	GraphPad Software	https://www.graphpad.com/
STAR 2.5.2b	Dobin et al., 2013[50]	https://github.com/alexdobin/STAR
Bowtie2	Langmead and Salzberg, 2012[57]	http://bowtie-bio.sourceforge.net/bowtie2/index.shtml
SAMtools v1.3.1	Li et al., 2009[51]	http://www.htslib.org/
HOMER v4.11.1	Heinz et al., 2010[52]	http://homer.ucsd.edu/homer/
org.Mm.eg.db v3.8.2	Bioconductor	https://bioconductor.org/packages/release/data/annotation/html/org.Mm.eg.db.html
R v3.6.3	CRAN	https://cran.r-project.org/bin/
Metascape	Zhou et al., 2019[54]	https://metascape.org/gp/index.html

(*Continued on next page*)

Continued

REAGENT or RESOURCE	SOURCE	IDENTIFIER
Cell Ranger	10x Genomics	https://www.10xgenomics.com/
Seurat v4.0	CRAN; Satija et al., 2015[58]	https://satijalab.org/seurat/ https://cran.r-project.org/web/packages/Seurat/index.html
Adobe Photoshop v13.0.1	Adobe Inc.	https://www.adobe.com/
Ingenuity Pathway Analysis	QIAGEN	https://www.qiage.com
DESeq2	Bioconductor; Love et al., 2014[53]	https://bioconductor.org/packages/release/bioc/html/DESeq2.html
Other		
Lymphoprep™	Axis-Shield	1,114,545
human CD14 magnetic beads	Miltenyi Biotec	130-050-201
Neutrophil Isolation Kit, mouse	Miltenyi Biotec	130-097-658
Pan B Cell Isolation Kit II, mouse	Miltenyi Biotec	130-104-443
KAPA mRNA HyperPrep	Roche Diagnostics	8,098,123,702
Disuccinimidyl Glutarate	Thermo Fisher	20,593
NEBNext® Ultra™ II Q5® Master Mix	NebioLabs	M0544
RNeasy® Mini kit	QIAGEN	74,106
ImmPACT® AMEC Red Substrate Kit	Vector Laboratories	SK-4285
VECTASTAIN ABC elite	Vector Laboratories	PK-6100
Avidin/Biotin Blocking Kit	Vector Laboratories	SP-2001
iScript™ cDNA Synthesis Kit	Bio-Rad	1,708,890
Fast SYBR™ Green Master Mix	Applied Biosystems	4,385,610
NE-PER™ Nuclear and Cytoplasmic Extraction Reagents	Thermo Fisher	78,833

RESOURCE AVAILABILITY

Lead contact

Further information and requests for resources and reagents should be directed to and will be fulfilled by Menno de Winther (m.dewinther@amsterdamumc.nl).

Materials availability

This study did not generate any new, unique reagents.

Data and code availability

- Sequencing data are deposited in the Gene Expression Omnibus (GEO) under the accession number: GSE193119.
- This paper does not report original code.
- Any additional information required to reanalyze the data reported in this paper is available from the lead contact upon request.

EXPERIMENTAL MODEL AND SUBJECT DETAILS

Animals

Mice

C57BL/6J *LysMcre*$^{-}$*Dot1l*$^{fl/fl}$ (WT) and *LysMcre*$^{+}$*Dot1l*$^{fl/fl}$ (KO) mice were derived by crossing mice with *loxP* sites flanking exon 2 of the *Dot1l* gene (*Dot1l*$^{fl/fl}$) with mice *Lyz2*-Cre transgenic mice. *Dot1l*$^{fl/fl}$ mice were based on the Dot1Ltm1a(KOMP)Wtsi line generated by the Wellcome Trust Sanger Institute (WTSI) and obtained from the KOMP Repository (www.komp.org).[48] *LysMcre* crossbreeding was performed in our mice facility. Mice were housed at the Animal Research Institute Amsterdam UMC (ARIA) and all mice experiments were conducted after approval of the Committee for Animal Welfare (University of Amsterdam).

Atherosclerosis mouse model

±12-week-old female *Ldlr*$^{-/-}$ C57BL/6J mice were used to study atherosclerosis. A bone marrow transplantation (BMT) was performed using five male *LysMcre*$^{-}$*Dot1l*$^{fl/fl}$ (WT) and five *LysMcre*$^{+}$*Dot1l*$^{fl/fl}$ (KO) mice. Mice were housed at the Animal Research

Institute Amsterdam UMC (ARIA). Forty *Ldlr*$^{-/-}$ mice were randomly assigned to the two experimental groups (20 mice per group) in filter-top cages provided with antibiotics water (neomycin (100mg/L) and polymyxin B sulfate (60,000 U/L, Invitrogen) from 1 week before BMT for 6 weeks. *Ldlr*$^{-/-}$ mice were irradiated with 2 x 6 Gy total body irradiation on two consecutive days. Subsequently, irradiated mice received 5*10^6 BM cells intravenously from either 5 pooled *Dot1l* WT or KO mice, resuspended in RPMI 1640 (Gibco) with 5 U/ml heparin and 2% FCS (Gibco). Five weeks after BMT, mice were fed an HCD containing 16% fat (15% cocoa butter, 1% corn oil, 0.15% cholesterol; Altromin C1000 mod.) *ad libitum* for 9 weeks to stimulate atherogenesis. After 9 weeks of HCD, mice were killed and hearts were isolated and frozen in Tissue-Tek (Dako) for histology. Unfasted blood samples were drawn by cardiac puncture using 0.5 M EDTA (Invitrogen) coated needles and syringes. Fasted (4h) blood samples were drawn from the tail vein at week 0, 5, and 8 of the HCD for the cholesterol and triglyceride measurements. All animal experiments were performed at the University of Amsterdam and approved by the Committee for Animal Welfare of the Amsterdam UMC - Location AMC, University of Amsterdam.

Primary cell cultures

Bone marrow-derived macrophages

Bone marrow (BM) was isolated from the femurs and tibias of male and female mice by flushing. BM was cultured in RPMI 1640 containing 25 mM HEPES, 2 mM L-glutamine, 10% FCS, 100 U/mL penicillin, 100 μg/mL streptomycin (all purchased from ThermoFisher), and 15% L929-conditioned medium (M-CSF source) for 7-8 days. During differentiation, 1 μM of the DOT1L inhibitor SGC0946 (Sigma) was administered to the BMDMs. For LXR activation, BMDMs were incubated with 2μM GW3965 (Sigma) on day 7 for 17h. For SREBP inhibition, BMDMs were incubated with 10μM PF-429242 dihydrochloride (Sigma) to inhibit S1P (site 1 protease) on day 7 for 24h. Dimethyl sulfoxide (DMSO; Sigma) was used as a control for SGC0946, GW3965, and PF-429242 dihydrochloride. On day 8, BMDM were stimulated with or without 10 ng/mL LPS (from *Escherichia coli*; O111:B4; Sigma) or LPS + 100 U/mL IFN-γ (PeproTech) for 3 or 24 hours.

Peritoneal macrophages

±11-week-old male and female mice were injected (i.p.) with 3% thioglycollate (Fisher Scientific) to induce a sterile inflammation that attracts monocytes. Mice were killed by CO_2 asphyxiation after 4 days. Peritoneal cells were collected, from five mice per group, by flushing the peritoneum with ice-cold PBS. Peritoneal cells were cultured in RPMI 1640 containing 25 mM HEPES, 2 mM L-glutamine, 10% FCS, 100 U/ml penicillin, and 100 μg/ml streptomycin (Gibco). After 3 hours, floating cells were washed away and adherent cells, the macrophages, were stimulated with or without 100 ng/ml LPS (Sigma) for 24 hours. Thioglycollate-injected mice were not used for the scRNAseq experiment.

Human monocyte-derived macrophages

Buffy coats from 4 healthy anonymous donors (2 males and 2 females) were acquired from Sanquin Blood Supply (Amsterdam, the Netherlands). All the subjects provided written informed consent before donation. Monocytes were isolated through density centrifugation using Lymphoprep (Axis-Shield) followed by human CD14 magnetic beads purification using MACS separation LS columns (Miltenyi). Monocytes were seeded and subsequently differentiated to macrophages within 6 days in Iscove's Modified Dulbecco's Medium (IMDM) containing 50 ng/mL human M-CSF (Miltenyi), 10% FCS, 1% Penicillin/Streptomycin (Gibco) 1% L-glutamine (Gibco), and with the DOT1L inhibitor (1 mM, SGC0946, Sigma) or DMSO (Sigma) as control. The medium was refreshed after three days. After differentiation, macrophages were stimulated with or without 10 ng/mL LPS (Sigma) for 3 or 24 hours.

METHOD DETAILS

Flow cytometry

To measure protein expression, 1.5x10^5 BMDMs were seeded per well in a 96-well plate and stimulated with 10 ng/mL LPS or 100 U/mL IFN-γ (PeproTech) for 24 hours. After stimulation, macrophages were detached with TrypLE (ThermoFisher). Fc receptors were blocked with anti-CD16/CD32 (eBioscience) for 15 minutes at room temperature (RT). Fluorescent labeled antibodies targeting CD11b (eBioscience), F4/80 (eBioscience), CD64 (BioLegend), MHCII (Biolegend), and CD86 (eBioscience) were incubated for 20 minutes at RT (antibody details in Table S1). Labeled cells were resuspended in PBS with 0.5% BSA and 2.5 mM EDTA and measured on a Beckman Coulter CytoFLEX and analyzed with FlowJo software version 10.7.0. Debris and doublets were excluded using forward and side scatter. CD11b$^+$F4/80$^+$ cells were considered as macrophage. An example of the gating strategy to determine e.g. CD64, CD86, and MHC-II membrane expression is provided in the supplemental information (Figure S7A).

To measure H3K79me2 levels, 5x10^5 BMDMs were blocked with anti-CD16/CD32 (eBioscience) for 15 minutes at RT. Cell fixation and permeabilization were performed using a Fixation/Permeabilization solution (ThermoFisher) for 30 min on ice. Antibodies targeting H3K79me2 (1:200, clone NL59, Sigma) were incubated for 30 min in permeabilization buffer (ThermoFisher) with 0.25% SDS. Alexa Fluor 488 donkey anti-rabbit IgG (H+L; 1:1000; ThermoFisher) was used as a secondary antibody and incubated for 30 min. Labeled cells were further analyzed as described above.

To measure blood cell frequencies, blood was withdrawn from mice via tail vein incision using Microvette CB 300 K2 EDTA tubes (SARSTEDT) after 9 weeks of HCD. Plasma was separated from blood cells by centrifugation (10 min, 4°C, 2000 RPM). Red blood cells were lysed with 5 mL erythrocyte lysis buffer (8.4 g of NH_4Cl, 0.84 g of $NaHCO_3$ and 0.37 g EDTA per 1 L distilled water) for 15 min at RT. Subsequently, cells were washed with PBS, and Fc receptors were blocked with a CD16/CD32 antibody (1:100, eBioscience) in PBS with 0.5% BSA and 2.5 mM EDTA. Next, cells were incubated with antibody mixtures for 30 min at RT antibody (antibody

details in Table S1). Labeled cells were resuspended in PBS with 0.5% BSA and 2.5 mM EDTA and measured on a Beckman Coulter CytoFLEX and analyzed with FlowJo software version 10.7.0. The gating strategy to determine B cell and T cell percentages of $CD45^+$ cells (including $CD4^+$ and $CD8^+$ percentages of T cells) is provided in the supplemental information (Figure S7B). The gating strategy to determine monocyte (including $Ly6C^{low}$ and $Ly6C^{high}$ percentages of monocytes), neutrophil and eosinophil percentages of CD45+ cells is shown in Figure S7C.

Cell culture supernatant measurements

Human IL-1β and IL-8 cytokine concentrations were measured in the supernatant of hMDM with LPS stimulation by a multiplex assay kit (V-PLEX Custom Human Cytokine Proinflammatory Panel 1 from MSD). The assays were performed according to the manufacturer's protocol with an overnight incubation at 4°C. Data were acquired using a MESO QuickPlex SQ 120 plate reader (MSD) and analyzed with Discovery Workbench Software (v4.0, MSD). Secreted human IL-6 and IL-12/IL-23 (p40) cytokine concentrations of hMDM with LPS stimulation were determined with an enzyme-linked immunosorbent assay (ELISA) MAX set (BioLegend). Total plasma cholesterol and triglyceride levels were quantified by enzymatic CHOD-PAP and GPO-PAP methods (Roche). Alanine aminotransferase (ALT) levels were quantified using an ALT Activity Assay (Sigma) according to the manufacturer's protocol. Secreted IFN-β concentrations of 3 and 24 hours LPS stimulated BMDMs were determined using the mouse IFN-β DuoSet enzyme-linked immunosorbent assay (ELISA) kit (R&D Systems) according to the manufacturer's protocol.

Real-time PCR

RNA was isolated using the RNeasy Mini Kit (QIAGEN). 200 ng RNA was used for cDNA generation with iScript (Bio-Rad). qPCR was performed with 2 ng/μL cDNA using Fast SYBR Green (ThermoFisher) on a ViiA7 PCR machine (Applied Biosystems). *Dot1l* exon 2 mRNA expression was normalized to the mean of the two housekeeping genes *Actb* and *Gapdh (or Actb and Ppia)*. Primer sequences are shown in Table S2.

Neutrophil and B cell isolation

BM neutrophils (n = 6 biological replicates per group) and splenic B cells (n = 5 biological replicates per group) were isolated using negative selection kits (Miltenyi Biotec) according to the manufacturer's instructions. As described above, RNA was isolated, cDNA was synthesized, and *Dot1l* KO efficiency was determined by qPCR.

Bulk RNA sequencing

RNA was isolated from BMDMs and HDMs using the RNeasy Mini Kit (QIAGEN) with DNase treatment. 700 ng RNA was used for Illumina library construction. RNA amplification, cDNA generation, and adaptor ligation were performed using the KAPA mRNA HyperPrep Kit (Roche) following the manufacturer's instructions. Samples were pooled, diluted to 10 nM, and sequenced single-end on an Illumina HiSeq 4000 system (Illumina) to a depth of ±20 million reads with a length of 50 base pairs.

H3K79me2 ChIP-seq

H3K79me2 ChIP-seq was performed as described previously.[49] Briefly, 10-20 million BMDMs were lifted using TrypLE (ThermoFisher) and crosslinked with 1% formaldehyde (ThermoFisher) for 10 min. Chromatin was pulled down overnight using an anti-H3K79me2 antibody (Clone: NL59, Merck). Illumina libraries were created from 10 ng ChIP chromatin using the KAPA HyperPrep (Roche) kit. Libraries were pooled to a concentration of 10 nM and sequenced single-ended on an Illumina HiSeq 4000 instrument (Illumina) to a depth of ±40 million 50 bp reads per sample.

SREBP1/2 ChIP-seq

SREBP1/2 ChIP-seq was performed as described previously.[35] 30 million BMDMs were crosslinked in 2mM Disuccinimmidyl Glutarate (Pierce) and 1% formaldehyde. BMDMs were resuspended in swelling buffer (10 mM HEPES/KOH pH7.9, 85 mM KCl, 1 mM EDTA, 0.5% IGEPAL CA-630, 1x protease inhibitor cocktail, 1 mM PMSF) and incubated on ice for 5 minutes. Cells were spun down and lysed in 130 μl RLNR1 lysis buffer (20 mM Tris/HCl pH7.5, 1 mM EDTA, 0.5 mM EGTA, 0.1% SDS, 0.4% Na-Deoxycholate, 1% NP-40 alternative, 0.5 mM DTT, 1x protease inhibitor cocktail, 1 mM PMSF) and chromatin was sheared by sonication in a 96 Place microTUBE Rack (Covaris cat#500282) using a Covaris E220 for 18 cycles with the following setting: time, 60 seconds; duty, 5.0; PIP, 140; cycles, 200; amplitude, 0.0; velocity, 0.0; dwell, 0.0. Samples were recovered and spun down at max speed, 4°C for 10 minutes. 1% supernatant was taken as input DNA and remaining supernatant was transferred to PCR strips and brought up to a volume of 200 μl using RLNR1 lysis buffer (20 mM Tris/HCl pH7.5, 1 mM EDTA, 0.5 mM EGTA, 0.1% SDS, 0.4% Na-Deoxycholate, 1% NP-40 alternative, 0.5 mM DTT, 1x protease inhibitor cocktail, 1 mM PMSF). 30 μl Dynabeads Protein A/G coated with the indicated antibodies for SREBP1/2 (antibody details in Table S1) were added to the sample, and immunoprecipitation was carried out at 4°C overnight. Beads were then collected using a magnet and washed with 175 μl ice-cold buffer as indicated by incubating samples on ice for 3 minutes: 3 times RLNR1 lysis buffer (20 mM Tris/HCl pH7.5, 1 mM EDTA, 0.5 mM EGTA, 0.1% SDS, 0.4% Na-Deoxycholate, 1% NP-40 alternative, 0.5 mM DTT, 1x protease inhibitor cocktail, 1 mM PMSF), 6 times LiCl-NR1 buffer (10 mM Tris/HCl pH7.5, 250 mM LiCl, 1 mM EDTA, 0.7% Na-Deoxycholate, 1% NP-40 alternative, 1x protease inhibitor cocktail, 1 mM PMSF), 3 times TET (10 mM Tris/HCl pH 8.0, 1 mM EDTA, 0.2% Tween-20, 1x protease inhibitor cocktail, 1 mM PMSF), and 1

time IDTET (10 mM Tris/HCl pH 8.0, 0.1 mM EDTA, 0.2% Tween-20, 1x protease inhibitor cocktail, 1 mM PMSF). Bead complexes were resuspended in 25 μ

l TT (10 mM Tris/HCl pH 8.0, 0.05% Tween-20, 1x protease inhibitor cocktail) and sequencing libraries were prepared on-bead as described below. ChIP libraries were prepared while bound to Dynabeads using NEBNext Ultra II DNA Library preparation kit. Libraries were eluted and crosslinks reversed by adding to the 46.5 μl NEB reaction, 20 μl water, 4 μl 10% SDS, 4.5 μl 5 M NaCl, 3 μl 0.5 M EDTA, and 1 μl 20 mg/ml proteinase K, 1 μl RNase E, followed by incubation at 55°C for 1 hour and 65°C for 2 hours to overnight in a thermal cycler. Dynabeads were removed from the library using a magnet and libraries were cleaned by adding 2 μl SpeedBeads 3 EDAC in 61 μl 20% PEG 8000/1.5 M NaCl, mixing well, then incubating at RT for 10 minutes. SpeedBeads were collected on a magnet and washed two times with 150 μl 80% ethanol for 30 seconds. Beads were collected and ethanol was removed following each wash. After ethanol wash, beads were air-dried and DNA eluted in 13 μl 10 mM Tris/HCl pH 8.0 and 0.05% Tween-20. DNA was amplified by PCR for 14 cycles in a 25 μl reaction volume using NEBNext Ultra II PCR master mix and 0.5 μM each Solexa 1GA and Solexa 1GB primers. PCR amplified libraries were size selected 200-500 bp using gel extraction using 10% TBE acrylamide gels. Libraries were single-end sequenced using a NextSeq 500 to a depth of 10-20 million 75 bp reads per sample.

Western blot

Cell lysis and extraction of nuclear protein fractions were performed using NE-PER Nuclear and Cytoplasmic Extraction Reagents (ThermoFisher). Protein lysates were mixed with Bolt sample reducing agent (ThermoFisher) and Bolt LDS sample buffer (ThermoFisher) and heated at 95°C at 500 RPM for 10 minutes. Next, protein lysates and a Spectra™ Multicolor Broad Range protein ladder sample (ThermoFisher) were loaded on a Bolt 4-12% Bis-Tris plus gel (Invitrogen) and ran at 100V for 1-1.5 hours in Bolt™ MOPS SDS running buffer (ThermoFisher). Samples were transferred to a nitrocellulose membrane in NuPAGE transfer buffer (Invitrogen) at 20 V for 1 hour. Next, the membrane was blocked with 5% milk in TBST for 1 hour at RT. Subsequently, the membrane was incubated with anti-SREBP2 (1:1000, Sigma) for 40 hours or with anti-histone H3 (1:5000, Cell Signalling) for 16 hours, both in 1% milk at 4°C. Antibody details are shown in Table S1. After washing the membranes with TBST, the membranes were incubated with a secondary goat-anti-rabbit poly HRP (1:1000, ThermoFisher) for 1 hour at RT. The membranes were washed again with TBST and incubated with the Pierce ECL substrate (ThermoFisher). Images were acquired using a chemiluminescence imaging system (Amersham ImageQuant 800 Cytiva). The relative intensity of N-SREBP2 was calculated by using histone H3 as a housekeeping protein and the ImageJ software.

Bioinformatics bulk RNA-seq

Reads were aligned to the mouse genome mm10 or human genome hg38 by STAR 2.5.2b with default settings.[50] BAM files were indexed and filtered on MAPQ>15 with SAMtools (v1.3.1).[51] Raw tag counts and reads per kilobase million (RPKM) per gene were summed using HOMER2's analyzeRepeats.pl script with default settings and the -noadj or -rpkm options for raw counts and RPKM reporting.[52] Differential expression was assessed using the DESeq2 Bioconductor package in an R 3.6.3 environment with gene expression called differential with an FDR<0.05.[53] Pathway enrichment analysis was performed using Metascape in which only Gene Ontology (GO) pathways were included.[54] Upstream regulator analysis was performed using Ingenuity Pathway Analysis (IPA) software (QIAGEN). Motif analysis was performed using the HOMER tool findMotifs.pl.

Bioinformatics H3K79me2 ChIP-seq

Reads were aligned to mouse genome mm10 using HISAT2. HOMER (v4.11.1) findPeaks was used for H3K79me2 peak calling with the setting -style histone.[52] Merged peak files were created using bedtools (v2.27.0) merge, and read coverage under peaks was calculated using coverageBed.[55] Merged peak files were combined with coverage files using bedtools unionbedg. ChIPseeker (v1.20.0) was used for peak annotation in an R 3.6.3 environment.[56] The methylation score was calculated by counting reads in a 3 kb window around the TSS. TSS regions were annotated by org.Mm.eg.db (v3.8.2). The UCSC genome browser was used for the visualization of generated ChIP-seq tracks (http://genome.ucsc.edu).

Bioinformatics SREBP1/2 ChIP-seq

Reads were aligned to mouse genome mm10 using Bowtie2.[57] SREBP1/2 binding sites were called with MACS2 using -q 1e-6. Genomic distribution of SREBP1/2 binding sites was determined using an in-house script yielding a list of 8056 genes with SREBP1/2 bound at the promoter (between 500 and -250 bp of the TSS). The significance of the overlap between SREBP1/2 bound and downregulated genes after DOT1L inhibition was computed using a hypergeometric test.

scRNAseq of atherosclerotic aortas

Atherosclerotic aortas were cut underneath iliac bifurcation and perfused slowly with PBS to remove blood cells. Subsequently, perivascular fat was removed using a microscope. Aortas were chopped and digested in an enzyme solution containing collagenase type I (3.6 g/L, Sigma), collagenase type XI (10 mg/L, Sigma), Hyaluronidase (15 mg/L, Sigma), and DNase I (Invitrogen) in RPMI 1640 with 5% FCS and 1% Penicillin/Streptomycin (Gibco) and incubated at 37°C for 50 min. Digested aortas were poured through a 70 μm cell strainer (Falcon). Three-till-ten aortas per group were pooled to create 2 pools per genotype. Aortic cells were centrifuged at 1300rpm

at 4°C for 10 min and Fc-receptors of aortic cells were blocked using anti-CD16/CD32 (eBioscience) for 15 minutes at RT. Cells were labeled with anti-CD45 (1:400, 20 min, RT, Biolegend). Before sorting, cells were poured through a 50uM filter, and dead cells were labeled using DAPI (0.2 μl/mL, ThermoFisher). Living $CD45^+$ cells were sorted with a FACSAriaIII (BD Biosciences) using an 85 μm nozzle. Sorted cells were collected in tubes containing RPMI 1640 with 20% FCS. Sorted cells were centrifuged (1300rpm, 4°C, 10 min) and resuspended in PBS + 0.04% BSA. $12*10^4$ sorted cells per group were used for the construction of a barcoded library using a Chromium Controller (10x Genomics). Libraries were sequenced on an Illumina HiSeq4000 platform. Data were analyzed and visualized using Cell Ranger (10x Genomics) and Seurat v4.0 in an R 3.6.3 environment.[58] Cells were filtered using the following conditions: nFeature_RNA > 200, nFeature_RNA < 7500, and percent.mito < 0.1. Unsupervised clustering on the remaining 4140 WT and 4250 KO cells identified 18 different clusters (dims = 1:20, resolution = 0.5, Figure S6A). Macrophage subsets were identified by the expression of *Ptprc*, *Cd68*, *Adgre1*, and *Mafb*, and the absence of *Cd3d* and *Cd79a* (Figure S6B). Macrophages were reclustered and further annotated via cluster marker identification and expression levels (differentially expressed genes) for each of the macrophage clusters and confirmed by literature (Figure 7B).

Histochemistry

Aortic roots were cut in 7 μm sections on a Leica CM3050S cryostat at -20°C. To measure plaque size, sections of every 42 μm were stained with Toluidine Blue (0.2 % in PBS, Sigma-Aldrich). To determine collagen content Sirius Red staining was performed (30 min, 0.05 % Direct Red in saturated picric acid, Sigma). For immunohistochemistry slides were fixed in acetone and blocked with Avidin/Biotin Blocking Kit (Vector Laboratories). To label monocytes and macrophages, sections were incubated with MOMA-2 (1:4000, Bio-Rad). For T cells, anti-CD3 (1:200, Bio-Rad), for B cells, anti-B220 (1:200, eBioscience), and for neutrophils, anti-Ly6G (1:200, BD Biosciences) was used. Biotin-labeled rabbit anti-rat antibody (1:300, Dako) was used as the secondary antibody (antibody details in Table S1). The signal was amplified using the ABC kit (Vector Laboratories) and visualized with the ImmPACT AMEC Red Peroxidase Substrate kit (Vector Laboratories). The necrotic area was determined by our animal pathologist using the Toluidine Blue stained sections including a correction for total plaque size. The total lesion area was calculated by the sum of the three valves per mouse. Images were obtained using a Leica DM5500B microscope and quantified using Adobe Photoshop (v13.0.1).

QUANTIFICATION AND STATISTICAL ANALYSIS

Bar graph data show the mean and include individual data points presenting each sample. Outliers were identified with the ROUT method with Q=1% and subsequently removed. Data were further analyzed by one-way ANOVA, two-way ANOVA, Kruskal-Wallis tests, two-tailed (un)paired t-test, or Mann-Whitney test after checking for normal distribution and equality of variance using GraphPad Prism 9.1.0 (GraphPad Software). Tukeys and Sidaks multiple correction tests were applied when necessary. $p<0.05$ was considered significant.